Quantifiable analysis of the failure of advanced carbon fibre composite structures leading to improved safety factors

Anthony R Bunsell, Alain Thionnet

Version of Record: https://www.sciencedirect.com/science/article/pii/S0079642520301171
Manuscript_32f9ab79f817e17edcd06ba720014372

Quantifiable analysis of the failure of advanced carbon fibre composite structures leading to improved safety factors

Anthony R. Bunsell[a,*], Alain Thionnet[a,b]

[a] *MINES ParisTech, PSL - Research University, MAT - Centre des Matériaux, CNRS UMR 7633 BP 87, 91003 Evry cedex, France*
[b] *Université de Bourgogne, Mirande, Dpt. IEM, BP 47870, Dijon, France*

Abstract

The increasing use of advanced composite materials means that they must now be considered as major materials for a wide variety of structures some of which will be in service for decades. There is therefore an important need to be able to quantify damage accumulation leading to failure in these materials particularly as they are often used in extreme situations for which failure must be avoided. This review shows how damage accumulation in many major composite structures is dominated by fibre failure but that the viscoelastic nature of the matrix induces time effects including delayed failure. It is shown that damage accumulation can be quantitatively modelled using a multi-scale approach linking damage at the fibre level to the overall reliability of the structure. The structures of particular interest are composite pressure vessels. At the microscopic level it is necessary to identify a representative volume element which includes all the processes which govern composite behaviour and failure. In this way the macroscopic loading of the composite structure can be evaluated at every point and overall behaviour qualitatively assessed. This allows the effects of loading to failure to be quantitatively calculated as well as the effects of loading at a constant level for long periods. It is shown that failure occurs when clusters of fibre breaks reach a critical level as has been observed experimentally. The effects of speed of loading and long term failure have also been observed experimentally as predicted by the simulations of structures including filament wound carbon fibre composite pressure vessels. This leads to the quantitative analysis of intrinsic safety factors for advanced composite structure based on a knowledge of the physical damage processes involved.

Keywords: fibre break, multiscale model, time dependent load, type IV cylinders, safety factor

*Corresponding author. Tel: +33 1 60 76 30 64
Email address: anthony.bunsell@mines-paristech.fr (Anthony R. Bunsell)

1. Introduction

High performance carbon fibres, based on polyacrylonitrile (PAN) precursors, were first developed at the Royal Aircraft Establishment in Farnborough in England in the mid-1960s and initially commercialised in 1967 by Courtaulds [1] [2]. Production of carbon fibres began in Japan in the early 1970s. Both the organisations in England have been merged with others and have lost their identities but the development of carbon fibres is of great significance, particularly for the forthcoming hydrogen economy. In the early 1970s the world production capacity of carbon fibres was less than ten tons and initial applications for the fibres and their composites were for military planes and sports goods. It is estimated that the world market capacity for carbon fibres in 2020 is around 240,000 tons. Although, for the aerospace industry, their composite materials have become to be seen as classical, standard materials, it is outside that industry that the fastest rate of growth and the biggest market can be found. Pressure vessels made of carbon fibre reinforced composites are the biggest single market for carbon fibres and these vessels are used to store both natural gas and increasingly hydrogen. The pressures are very high with in-service pressures for hydrogen being typically 70 MPa or 700 atmospheres.

Advanced composites are often used for structures for which traditional materials are not ideal or even suitable. These applications often require extreme properties of strength, stiffness combined with low weight and more often than not, great reliability is required as unforeseen failure could have dramatic and costly consequences. Nevertheless international standards for structures are most often based on traditional materials as, in the case of pressure vessels, there are ample anecdotal reports of failures of metal vessels going back two hundred and fifty years, since the beginning of the industrial revolution. Developments in the understanding of failure processes in metals have supported a deep understanding of their mechanisms of failure which have led to quantifiable techniques for determining safety factors for metallic structures. All too often these standards have been used to define tests for evaluating behaviour of composite structures, such as composite pressure vessels, but with little or no justification based on the physical processes involved in their failure. An example is the proof testing of pressure vessels: the standard test is to over pressurise the vessel by 50% compared to the maximum in-service pressure. If the vessel does not break it is considered good to continue in service. At first sight this seems reasonable; if it does not break at a higher load why should it fail at a lower load? Metals fail by crack propagation and the stress concentration at the tip of the crack controls it. On overloading, the stress at the crack tip causes the material to locally deform plastically so that such a metal pressure vessel, after successfully surviving the test, will have any incipient cracks blocked, under in-service conditions,

by plastic zones developed during the test control. Fibre reinforced composites do not fail like that. The fibres making up the composite show great scatter in failure loads but their breakage controls the strength of the composite structure. The development of clusters of fibre breaks eventually cause failure and an analogy could be made with the development of critical cracks in a metal but the way the fibre breaks in composites are formed is very different. When enough of the fibres are broken the composite fails. Fibres such as carbon or glass are elastic so that overloading will immediately provoke further fibre breaks leading to the structure being closer to failure than before the test which provides in addition no information on residual lifetimes. As a result the proof test for metal structures is less than desirable for advanced composite pressure vessels.

This paper deals with the development of the understanding of the physical mechanisms which control both the short and long term behaviour, mechanical properties and failure mechanisms of advanced composite material structures through both experimental methods and computer simulation and proposes means of quantifying safety factors, for structures such as composite pressure vessels, based on physical processes.

2. Carbon fibres and their composites

The carbon-carbon bond is very strong (4000 kJ/mole), the strongest in nature, which accounts for the remarkable properties of carbon fibres. Carbon is the sixth element in the Periodic Table which means that it has lower density than most other materials. The manufacture of carbon fibres leaves open the possibility of producing a wide range of carbon fibre types; some pitch based carbon fibres have a Young's modulus of 935 GPa and so approach the upper limits of stiffness which are physically possible. The carbon fibres in widest use however are PAN based carbon fibres which combine handleability with cost and their Young's moduli of the most widely used carbon fibres are typically in the range 230 to 295 GPa with most structures using fibres having the former modulus for reasons of cost. This is coupled with strains to failure of up to and above 2% and strengths typically around 5 to 7 GPa. The fibres are fine having diameters in the range from five to seven microns for PAN based carbon fibres and up to eleven microns for pitch based carbon fibres. The most widely used carbon fibres have diameters around seven microns. The strong covalent bonds between the carbon atoms in the fibres results in elastic behaviour under tension. This should be noted as it implies no plastic deformation or creep of carbon fibres at room temperature. Single carbon fibres tested under cyclic loads do not appear to fail by a fatigue process or stress corrosion at room temperature [3].

Carbon fibres are most often used embedded in a resin matrix and although there are many

resins which are used the most widely used is epoxy resin which typically has a Young's modulus of up to 4 GPa.

The most efficient way of exploiting the properties of fibres in composite form is in a unidirectional composite in which all the fibres are aligned parallel to the loading direction. A simple law of mixtures shows that with a typical fibre volume fraction for a long fibre composite of 60% the matrix supports approximately only 1% of the applied load in the fibre direction. The fibres therefore dominate the behaviour of such a composite and this led to the assumption that the composite would behave elastically with no time dependent or plastic deformation properties. This is a satisfactory conclusion as it removes the need to understand the effects of loading history on the behaviour of a composite structure. Unfortunately it may be satisfying but it is wrong.

Early in the exploration of carbon composite behaviour it was found that cyclic loading of unidirectional carbon fibre composites loaded in the fibre direction, with a constant load amplitude, led to increasing damage but with a decreasing rate of damage as the loading proceeded [4]. Damage was monitored by acoustic emission. Further tests on these specimens revealed that the acoustic emission was coming from fibres which were breaking. Further tests on internally pressurised carbon fibre composite rings and also filament wound pressure vessels revealed exactly analogous behaviour. Later similar results were shown for unidirectional specimens under constant load, which removed any contribution due to the hysteresis effects induced by plastic deformation [5] [6] [7].

Figure 1 illustrates this loading process and Figure 2 shows that if the load is increased monotonically and then held constant the damage continues to increase, as shown by the vertical part of this experimental curve. Resuming the monotonic loading initially results in little damage until the extrapolated initial curve is reached. This showed that a time effect existed which resulted in damage occurring during sustained loading which would have occurred in a monotonic test at higher loads.

As the carbon fibres were elastic it became clear that it was the viscoelastic behaviour of the matrix which accounted for this observation. It can be noted that the viscoelastic effects of the matrix have been first shown by Lifschitz and Rotem [8] and much more recently by Chou *et al.* [9]. Loading carbon fibre composites in their most stable form, that is unidirectional loaded parallel to the fibres, leads to increasing damage even under constant loads. Recently this has been shown in dramatic form when loading unidirectional carbon fibre composites under a constant load very near their tensile breaking load. In this way the usual slow damage accumulation could be accelerated

to result in failure in just a few hours (Fig. 3). Under a steady load the composite accumulated damage, as is seen at lower load levels in plate and also filament wound structures, but eventually reached a point where the damage accelerated and led to failure. These materials age as does everything. In the early days of carbon fibre composites this was not considered relevant for the types of structures being made however today, with increasing numbers of civilian applications, such as pressure vessels, for which lifetimes, measured in decades, are required and failure avoided at all cost, damage accumulation over time has to be considered. It has become clear that to correctly understand the behaviour of the composites it is not sufficient to assume elastic behaviour but the viscoelastic contribution of the matrix must be included in any analysis.

In any carbon fibre composite there are most probably millions of fibres arranged in different directions. The most common arrangement is of stacks of unidirectional layers placed on top of one another with the layers arranged in a variety of directions. This is to overcome the inconvenience of the anisotropy of single layers. Other arrangements include weaving the fibres used in the layers or braiding them. In the case of a pressure vessel the filament winding process means that the fibres are wound on geodesic paths and therefore when the vessel is pressurised the fibres are primarily locally subjected to tensile forces as in a unidirectional composite. The fibres are wound at an angle to the long axis going around the hemispherical ends and also at right angles to this axis to reinforce the vessel in a circumferential direction. It is this latter reinforcing arrangement which determines the burst pressure. This means that locally the structure, within a given, layer can be likened to a unidirectional composite and tests on such vessels reveal that they show exactly analogous behaviour.

Carbon fibres typically used to make a composite structure, taken from a strand of perhaps twenty four thousand fibres show considerable scatter in their tensile properties. The variation in strength of carbon fibres can be described by Weibull statistics and the scatter is quantified by the Weibull modulus. The greater the value of this modulus the less scatter is found with a given material. Carbon fibres, like most fibres, typically have a low Weibull modulus, between 3 and 4 [10]. Fibres are therefore broken during the manufacturing process of composites and also during initial loading as some are weak. This results in broken fibres existing in composite structures before they enter in service. It will be shown that these points of fibre breaks can initiate further fibre breaks, even under unvarying loads and some sites can eventually cause failure of the structure. This variation in properties must be understood and its effect on the ultimate composite properties included in simulations of composite structures. The small diameters of carbon fibres means that they cannot be placed in a regular array in a composite so that, although the overall

fibre volume fraction is fixed by the manufacturing process, locally this volume fraction can vary greatly. This has to be understood in determining the characteristics of a composite structure.

3. Failure processes in unidirectional composites

As mentioned above many composite structures are made of rovings of carbon fibres arranged in layers with the fibres in the plies organised in various directions. In such a cross-plied structure a number of failure processes are possible, such as matrix cracking or fibre-matrix debonding, but always in the direction of the fibres it is their behaviour which determines the failure of a particular ply. In the case of a filament wound structure, such as a pressure vessel, the fibres are subjected primarily to tensile forces due to the pressure and ensure the integrity of the structure. The circumferential layers are usually designed to control ultimate burst strength. The fibres do experience compressive forces across the plies but within the range of pressures encountered by pressure vessels these compressive forces have been shown not to cause fibre failure, which, if it did, occur would weaken the structure [11].

The stress field in a particular fibre in a composite under load is affected by its proximity with any nearby broken fibre which may exist. Intact fibres neighbouring a fibre break will have to take up the load which the broken fibre had been supporting before its break. This phenomenon results in the redistribution of loads from the broken fibre to, particularly, neighbouring intact fibres. It can also be amplified by the existence of debonding between the broken fibre and the matrix. The effect is further amplified over time by the viscous nature of the matrix allowing the matrix to relax locally around a fibre break with the result of increasing loads on neighbouring intact fibres. For simplification the behaviour of the matrix will be considered in this paper to be isotropic and linearly viscoelastic.

In order to simulate the behaviour of a real composite structure the above physical phenomena must be included in including the random nature of the arrangement of the fibres.

4. Introduction to the modelling of a carbon fibre structure

The structure which will be considered in this paper will be initially the unidirectional carbon fibre composite loaded in tension which will lead to the simulation of filament wound pressure vessels. Several manufacturing processes have been used to make the UD laminates including compression moulding, filament winding and pultrusion. The various techniques had different advantages and disadvantages with the pultruded specimens considered to be the best for obtaining unambiguous

results concerning the intrinsic damage processes occurring in pressure vessels. The objective will be to show how an understanding of the failure processes which occur in a pressure vessel can be quantitatively evaluated in terms of the failure of unidirectional composites at the microscopic scale. This will be achieved by computer modelling relating the behaviour of the whole structure to the microstructure on the scale of the fibres. This must be achieved with simulations based on physical processes but also by using an efficient modelling approach so as to limit calculation times. The result is a much improved understanding of the failure processes and the means to optimise the design of composite pressure vessels whilst retaining acceptable safety margins and reducing their cost of manufacture.

The results at the microscopic level will be included in the calculation at the scale of the complete industrial structure which is the goal. However such a calculation is immediately confronted with the problem of passing from the microscopic to the macroscopic. It is not possible to envisage basing the Finite Element calculation of the whole structure by simulating the behaviour of all the fibres in the composite. This would entail impossibly long and expensive calculation times because of the very large number of fibres making up the structure and the very large numbers of degrees of freedom involved.

A multi-scale process is potentially the solution to this problem as it is capable of both addressing the finest parts of the structure, together with their physical characteristics, and describing the whole structure with reasonable calculation times.

Such a two-scale approach has been used in tackling this problem and the approach is described as FE^2 and has been used in the works of Feyel [12], Thionnet [13] and Souza *et al.* [14].

Despite the increasing power of calculators it is clear, however, that without taking into account the specificities of the mechanisms studied or other details of the processes involved the FE^2 multi-scale process would not be powerful enough to result in calculation times acceptable for practical use, so the process has had to be simplified. In order to do this only the most conservative conditions will be considered which means that the results will also be slightly conservative. However, given the nature of the structures considered for which failure must be avoided this is considered a desirable outcome.

The multi-scale process, even simplified, will allow the relations between the microscopic scale and the scale of the structure, described as the macroscopic scale, to be understood. For that, at the macroscopic scale, it is necessary to define the minimum volume of the composite which

is statistically representative of this material at the macroscopic scale: this volume is called the Representative Volume Element (RVE).

Basically and in the most general manner a multi-scale process consists of applying the evaluation of the macroscopic fields (usually stresses and strains) at each point in the macroscopic structure experienced by the RVE, described at the microscopic scale and existing under every macroscopic point in the structure.

As a first step, after the description of the physical processes implicit at the microscopic scale, it is the precise description of the RVE and its microstructure which must be made. It is this which will be included in the model as well as the analyses of the physical phenomena which will be considered.

The model which has been used here has been developed based on the understanding that fibre breaks are the primary failure mechanism in composite structures by Blassiau, Bunsell and Thionnet [15], [16], [17], [18]. It is solidly based on earlier studies by many researchers into the failure of unidirectional composites which have included analytical, statistical and less often numerical approaches with occasional considerations of the viscoelastic nature of the matrix. The following, non-exhaustive list of studies merit being cited: Rosen [19], Cox [20], Zweben [21], Hedgepeth [22], Ochiai *et al.* [23], Curtin [24], [25], Ibnabdeljalil and Curtin [26], Goree and Gross [27], Harlow and Phoenix [28], [29], Scop and Argon [30], [31], Kong [32], Batdorf [33], [34], Nedele and Wisnom [35], [36], Hedgepeth and Van Dyke [37], Baxevanakis [38], Landis *et al.* [39], [40], Phoenix *et al.* [41], [42], [43], [44], Wisnom [45], Van Den Heuvel *et al.* [46], [47], Lipschitz and Rotem [8], Lagoudas *et al.* [48], Beyerlein *et al.* [49]. The above studies have led to an increasing understanding of failure processes in composites and inspired the model used here. The present model is written at the scale of the fibre (microscopic scale) and included in a simplified [50]multiscale FE^2 approach [12] [13] which allows composite structure failure to be calculated. It has been validated at the microscopic scale [51] and at the macroscopic (structural) scale [9].

4.1. The stochastic nature of the fibre strength

As mentioned above the strengths of carbon fibres, σ_R, show a wide scatter which has to be described in a statistical manner. Tests made by Baxevanakis [38] and [15] on carbon fibres with different gauge lengths illustrate this phenomenon (Fig. 4). A two-parameters Weibull function $P_R(\sigma_R)$ can be used to describe this statistical characteristic of fibre failure:

$$P_R(\sigma_R) = 1 - e^{-(\frac{L}{L_0})(\frac{\sigma_R}{\sigma_R^0})^{m_{\sigma_R}}} \tag{1}$$

where σ_R^0 and m_{σ_R} are respectively the scale and the shape parameters of the Weibull function, L and L_0 are respectively the tested and the reference gauge lengths of the fibres.

The strength of a fibre varies along its length as failure is initiated by local microscopic defects. Within a structure, the value of the failure stress of a given fibre is then dependant on the considered point along the axis of the fibre, so that in the domain defining this structure, the function, denoted as $\sigma_R(M)$, giving a value of σ_R at the given point M defines a field of local fibre strength. Therefore, $\sigma_R(M)$ is implicitly a local quantity and in the following, the fibre strength should be understood as the local fibre strength. It should be also recalled that the fibre strength is the value of the force applied to the fibre when the fibre breaks divided by the cross section area at the point of failure of the fibre.

The model which is described here takes into account the random nature of the failure of fibres along their axes by using a Mont-Carlo process which will describe the failure stress field $\sigma_R(M)$.

4.2. The stochastic nature of the local fibre volume fraction

The fineness of the carbon fibres means that their organisation within a composite cannot be precisely controlled and as a consequence the overall distribution of the fibres in a (0°) carbon/epoxy laminate is never regular. This means that the local fibre volume fraction can vary widely. Microscopic image analysis (Fig. 5a) was performed on three (0°) carbon/epoxy specimens to highlight and quantify the variation of local fibre volume fractions within the composite [52]. Three specimens were cut from the same plate ($20cm \times 20cm \times 20cm$) of (0°) carbon/epoxy material and therefore were nominally identical. For each specimen, approximately 1700 observations were examined.

The statistical characteristic of the local fibre volume fraction V_f is clearly shown (Fig. 5b) as a cumulative probability distribution $P_V(V_f)$ defined with a two-parameter Weibull function:

$$P_V(V_f) = 1 - e^{-(\frac{V_f}{V_f^0})^{m_{V_f}}} \tag{2}$$

where V_f^0 and m_{V_f} are respectively the scale and the shape parameters of the Weibull function.

Within a structure, the overall fibre volume fraction is controlled during manufacture however the local fibre arrangement cannot be well controlled. The local fibre volume fraction has a random nature. In the developed model, this is taken into account at each point of the structure by a Monte-Carlo process.

4.3. The viscous nature of the matrix

The tensile tests conducted on unidirectional specimens by [4] showed that the acoustic emission activity, for the case of increasing monotonic loading, increased until the final failure of the specimen. It was shown that this acoustic activity could be directly related to the breakage of fibres for this type of specimen: the global load applied was supported by the fibres that were increasingly loaded during the test. They progressively broke during the increasing of the load.

Similar tests were conducted by Laroche [5] [6] [53] and Blassiau [15] [17], but for when the load was held at a given constant value. In this case, it could have been expected that, at the end of the increasing part of the load, the acoustic activity would stop. However this was not the case because fibres continued to break (Fig. 2, Fig. 3). The overall load remained constant but clearly the local load on some fibres increased causing their failure (Fig. 6). The explanation is that the load on each fibre neighbouring fibre breaks continued to increase even if the global loading was held constant because the surrounding matrix relaxed due to its viscosity, resulting in an increase in the local load supported by the fibres.

The evolution of the longitudinal strain of the specimen was found not to be measurable. As a consequence in the framework of the model the viscoelastic character of the matrix must be taken into account at the level of the constituents but can be neglected at the scale of the structure.

5. Description of the RVE. Definition of the framework associated with the microscopic scale and random local fibre volume fraction

Starting from the study of Baxevanakis [38] Blassiau [15] [16] [17] [18] identified (without a rigourous proof) the geometry and the microstructure of the Representative Volume Element (RVE) for the virgin material, which is considered undamaged and not to contain any broken fibres. Recently, Rojek [54] proved that this geometry is correct. The geometry is that of a parallelepiped with a length L and a square section with sides of h. (Fig. 7). Inside this geometry there are N fibres, noted as F_i $(i = 1, \ldots, N)$. All the fibres are considered to be identical, arranged in parallel and perfectly cylindrical with circular cross-sections. All fibres have therefore the same circular cross-section and diameter, and same cross-sectional area S_F. This corresponds closely with reality. It is also supposed that the fibres are regularly spaced in a periodic square format. This does not correspond to reality but will be justified later. The research of Baxevanakis [38] and Rojek [54] has shown that whatever the fibre volume fraction considered (but around 60%) the RVE has a length of L equal to 4 mm and contains $N = 32$ fibres. The value of h depends on

the fibre volume fraction and the fibre diameters. For fibres with diameters around 7 microns the value of h is then:

- $h = 0.050$ mm for a fibre volume fraction of $V_f = 0.64$;
- $h = 0.064$ mm for a fibre volume fraction of $V_f = 0.39$;
- $h = 0.092$ mm for a fibre volume fraction of $V_f = 0.19$.

For this geometry, defined at the microscopic scale, the fibres and the matrix are clearly represented and associated with the framework $R_y = (O_y, b_y)$ for which the base, which is taken to be orthonormal, is defined by $b_y = (\vec{y_1}, \vec{y_2}, \vec{y_3})$ and O_y the origin (Fig. 7). The longitudinal axes of the fibres are aligned with the vector $\vec{y_1}$ which defines the length of the parallelepiped. O_y is placed at the geometrical centre of one of the two square sections of the parallelepiped so that $\vec{y_1}$ is the normal vector and is directed towards the interior. The two other vectors $\vec{y_2}$ and $\vec{y_3}$ are such that they are orthogonal to the planes which define the other faces of the parallelepiped.

It is necessary at this point to discuss the hypothesis of the periodic arrangement of the fibres within the RVE. It is clear that this ideal periodic configuration within the RVE does not reflect what really occurs in a composite (Fig. 5). It is never found in a carbon fibre composite. So why consider this configuration when there is practically no chance of it being found in reality? The reason is that this configuration reflects the average configuration around which all others must oscillate. The results obtained (properties or other data) for the real configurations only vary as a second order with respect to the results obtained with the assumed periodicity [55]. Then, the RVE is clearly idealised and it is accepted that it does not directly correspond to the reality but it has been shown in other work that this has no significant impact on the result as a more realistic RVE only introduces secondary effects. The idealistic RVE used represents an averaged geometry around which other, random secondary, effects vary.

The choice taken here to include the random nature of the local fibre distribution (Section 4.2) has the effect that:

- a given fibre volume fraction is represented by a RVE which is exactly similar to that which is described above but that the dimensions of the RVE are adapted to the volume fraction considered;
- during the application of the process of multi-scale simulation a Monte-Carlo function is used to describe the randomness of the local fibre volume fraction at each point in the structure.

6. Creation of the multi-scale process

6.1. Notations for the scales and frameworks of the multi-scale process

Generally a multi-scale process links several scales to one another. Here two distinct scales are considered: that which sees the constituents (fibres and matrix) inside the RVE as distinct and separate continua and secondly the macroscopic scale which does not see them but considers the material as a single continuum. The first refers to the microscopic scale and the other the macroscopic scale. It is necessary to define a framework for each of these scales.

The geometry of the RVE has been previously identified as being a regular parallelepiped with a square cross-section in which $N = 32$ parallel fibres F_i $(i = 1, \ldots, N)$ are embedded. To this geometry at the microscopic scale is associated a direct framework $R_y = (O_y, \vec{y_1}, \vec{y_2}, \vec{y_3})$ where the vector $\vec{y_1}$ defines the axis of the fibres and $y = (y_1, y_2, y_3)$ designates the coordinates of a point P relative to this framework. The fields of displacement, stresses (supposed symmetrical) and deformation (linearised) are respectively noted as $\vec{v} = (v_i)_{i=1,2,3}$, $s = (s_{ij})_{i,j=1,2,3}$ and $e = (e_{ij})_{i,j=1,2,3}$. The values of these fields at a point P at time t are then respectively $\vec{v}(P,t)$, $s(P,t)$ and $e(P,t)$ of which the expression as a function of y is written in the same manner so as to avoid multiplying the notations: $\vec{v}(y,t) = (v_i(y,t))_{i=1,2,3}$, $s(y,t) = (s_{ij}(y,t))_{i,j=1,2,3}$ and $e(y,t) = e(\vec{v}(y,t)) = (e_{ij}(y,t) = \frac{1}{2}(\frac{\partial(v_i(y,t)}{\partial y_j} + \frac{\partial(v_j(y,t)}{\partial y_i}))_{i,j=1,2,3}$.

The framework for the macroscopic scale which is that of the structure is $R = (O, b)$ for which the orthonormal base is $b = (\vec{x}_1, \vec{x}_2, \vec{x}_3)$ and O the origin. The triplet $x = (x_1, x_2, x_3)$ designates the coordinates of a point M relative to this framework. The fields of displacements, stresses (supposed symmetrical) and strains (linearised) are respectively noted as $\vec{u} = (u_i)_{i=1,2,3}$, $\sigma = (\sigma_{ij})_{i,j=1,2,3}$ and $\varepsilon = (\varepsilon_{ij})_{i,j=1,2,3}$. The values of these fields at a point M at time t are then respectively $\vec{u}(M,t)$, $\sigma(M,t)$ and $\varepsilon(M,t)$ of which the expression as a function of x is written in the same manner so as to avoid multiplying the notations: $\vec{u}(x,t) = (u_i(x,t))_{i=1,2,3}$, $\sigma(x,t) = (\sigma_{ij}(x,t))_{i,j=1,2,3}$ and $\varepsilon(x,t) = \varepsilon(\vec{u}(x,t)) = (\varepsilon_{ij}(x,t) = \frac{1}{2}(\frac{\partial(u_i(x,t)}{\partial x_j} + \frac{\partial(u_j(x,t)}{\partial x_i}))_{i,j=1,2,3}$.

6.2. Organisation

6.2.1. Process

In order to set up the multi-scale process it is useful to precisely describe the organisation of the phenomena which will lead to the failure of the structure. It is on this organisation of the physical phenomena (which have been revealed by earlier investigations and experimental observations) that it becomes possible to construct the organisation of the multi-scale process. It should be recalled

that the goal is to take into account: the stochastic nature of fibre failure and local fibre volume fraction and the viscoelastic nature of the resin matrix.

From the start it is considered that the composite structure is made up of fibres which are not arranged in a regular manner. This random irregularity results in an inhomogeneous distribution of the fibre volume fraction within the structure (Section 4.2, Section 5), of which the associated RVE is itself made up of a regular array of fibres. This random characteristic is taken into account by attributing values to the local fibre volume fractions at each point M, through the use of a Monte-Carlo simulation. These values define the inhomogeneous character of the local fibre volume fraction, which is considered not to vary with time, through a scalar field $\mathcal{V}$ of which the value at point M is $\mathcal{V}(M) = V_f(M)$.

It is then considered that the unloaded structure is initially (at the beginning of loading at time t_0) in a given state of damage. At the macroscopic scale, this state is represented by a scalar field $\mathcal{D}$ of which the value in M at time t_0 is $\mathcal{D}(M, t_0)$. At t_0, it is usual (but not obligatory if the physical reality is different) to consider that at every point in the structure the material is undamaged.

The calculation can then be started, however at the macroscopic scale it is necessary to know at t_0 and at every point M of the structure the macroscopic behavioural properties of the material making up the structure. All these properties of varying mathematical natures (scalar, vectorial, second order tensorial) the number of which is given by p, are grouped in the following set $\mathbb{P}^C(M, t_0)$ containing and describing the p fields described as $\mathcal{P}_i^C(M, t_0)$ $(i = 1, ..., p)$. This set is noted: $\mathbb{P}^C(M, t_0) = \left\{\mathcal{P}_1^C(M, t_0), \ldots, \mathcal{P}_p^C(M, t_0)\right\}$. These properties are calculated at time t_0, by the solution, at the microscopic scale, of the problems of homogenisation applied to the RVE at point M, noted RVE(M), and the average operations on all of the solutions of these problems. The dependence with respect to M is due the local volume fraction being inhomogeneous and therefore the RVE is not the same at every point of the structure.

To obtain the quantities (properties or other variables) at the macroscopic scale from quantities (properties or other variables) at the microscopic scale is the homogenisation phase of the multi-scale process. This means that the properties at the microscopic scale, as well as the geometry of the RVE(M) are data.

If the behavioural properties are really inhomogeneous over all the structure in its initial state it is also the case for the failure properties, designated as $\mathcal{P}^R(M, t_0)$. In effect, our wish is to take

into account the random nature of the fibre strength along their axes. Thus, physically, that means, for example, that two neighbouring fibres, ostensively geometrically and behaviourally very similar and subjected to the same loads in the structure, do not break simultaneously or in the same place. This random nature is achieved in the simulation by attributing values of fibre strength, at each point M, through a Monte-Carlo process (Section 4.1). These values define therefore the inhomogenity of the failure strengths through a scalar field $\mathcal{P}^R$ for which the value at point M is $\mathcal{P}^R(M)$. It is convenient to note that $\mathcal{P}^R(M)$ is a field defined at the macroscopic scale: it is therefore clearly linked with the field σ_R of the fibre failure strengths (Section 4.1), but it is not in any case a priori directly the same field.

The initial state of the structure being clearly defined it is now possible to consider it under load and launch the multi-scale simulation. The load on the structure increases from zero and increases until it reaches a value at time t, noted $\mathcal{S}(t)$. Within the structure at the macroscopic scale there are stresses and strains imposed by the load, represented by the fields $\sigma(M,t)$ and $\varepsilon(M,t)$.

Due to the existence of these imposed macroscopic fields there exists within RVE(M) the states of stress $s(P,t)$ and strain $e(P,t)$ at time t at the point P at the microscopic scale. The calculation of the microscopic fields $s(P,t)$ and $e(P,t)$ induced by the macroscopic fields $\sigma(M,t)$ and $\varepsilon(M,t)$ is called the localisation step in the multi-scale process. The point P covers the geometry of the RVE(M) and notably the fibres and matrix. Noting s^{F_i} the restriction of the s field for the case where P is in the fibre F_i, and s^m the restriction of s where P is in the matrix. Thus for the specific case considered (the failure of fibre F_i at a point on its longitudinal axis), it is the average of the longitudinal component $s_{11}^{F_i}(P,t)$ over the cross section $S_{F_i}(y_1)$ situated on the abscissa y_1 which is of interest:

$$\langle s_{11}^{F_i}(P,t)\rangle(y_1,t) = \frac{1}{S_{F_i}(y_1)} \int_{S_{F_i}(y_1)} s_{11}^{F_i}(y_1,y_2,y_3,t)dy_2dy_3 \tag{3}$$

Because of the stochastic nature of failure of fibre F_i along its axis (Section 4.1), noted as $s_R^{F_i}(y_1)$, some fibres in the population are likely to break if the following condition is met:

$$\langle s_{11}^{F_i}(P,t)\rangle(y_1,t) \geq s_R^{F_i}(y_1)? \tag{4}$$

It should be noted that the values $s_R^{F_i}(y_1)$ applied at the microscopic scale at point P of the RVE(M), are values which come from $\mathcal{P}^R(M)$ constructed by the associated Monte-Carlo process.

Thus at point M at the macroscopic scale at instant t, a damaged material replaces the initially

undamaged material. The value in M, at t, of the scalar field $\mathcal{D}$ becomes $\mathcal{D}(M,t)$. This value obviously depends on the number of broken fibres in RVE(M) at time t. As for the initial undamaged state the behavioural properties $\mathcal{P}_i^C(M,t)$ $(i=1,...,p)$ are evaluated by a homogenisation step.

The time and loading continues to increase and the process described above is repeated until the structure fails. It is therefore necessary to clearly define the failure state of the structure which marks the end of the multi-scale process.

6.2.2. Stopping the process: failure of the structure

Generally a loading curve is defined with an objective of finding a quantity Q representative of the failure of a structure and more precisely, so as to exhibit a quantity Q for which the rate function of time or in another quantity becomes infinite.

For the case of monotonic loading until failure, a loading curve of a structure can be defined as a curve giving F, a quantity characteristic of the loading of the structure, versus U, a quantity characteristic of the response of the structure. This curve can be experimentally or numerically (using Fracture or Damage Mechanics) obtained. Depending on the considered case, the definition of the failure of the structure will be specific to each case and will not be the same. The (physical or experimental) failure of a structure is defined as the breakage into two parts of the structure (Fig. 8a). The failure point of a structure is the (experimental instability) point B_{INST_EXP} on the (experimental) loading curve where the failure appears. The failure load of a structure is defined as the value F_{INST_EXP} of F at the failure point. These concepts are very clear, experimentally, as well as in the framework of Fracture Mechanics, because in these cases the damage is clearly identified with the appearance of discrete surface where the displacement becomes discontinuous, cutting the structure into two parts.

In the case of Damage Mechanics, it is difficult to apply these definitions because in this framework damage never appears in a discrete way: the medium making up the structure is never physically cut. The concept of "the failure of a structure" should be "the failure of a structure is defined as the existence of a path-connected domain crossing the structure for which the medium is totally degraded": the point J marks this state on the simulated loading curve (Fig. 8b, point J), and point E illustrates the totally degraded but not cut material (Fig. 8, point E, grey area). The point J is then denoted as the Failure Point or Instability Point of the structure. This point is also characteristic of the fact that around it the simulated loading curve shows the beginning of a plateau indicating that the rate of U versus F becomes infinite.

To find an existing path-connected domain where the material is totally degraded with, as an objective, the identification of the point J is not easy. An easier, clear and reproducible method giving this point (or a very close one) is necessary. This is explained below.

The failure (instability) load F_{INST} of the structure is defined as the value of F at the intersection (Fig. 8b, point B) of the tangent of the instability plateau D_{INST} and the tangent D_{ELAS} at the origin of the loading curve. The characteristic displacement corresponding to F_{INST} on the simulated loading curve is denoted as U_{INST}. The characteristic displacement corresponding to F_{INST} on the tangent at the origin of the simulated loading curve is denoted as U_{SINST}. The value of F corresponding to U_{SINST} on the simulated loading curve is denoted as F_{SINST}. The point I is defined by the coordinates (U_{SINST}, F_{SINST}). The point J is defined by the coordinates (U_{INST}, F_{INST}).

In the case of the composite considered here (carbon fibre/resin), it is well known that the loading curve of structures made with such materials have the form shown in Figure 8: nothing significant indicates that the break will appear. This is a sudden-death failure. In other terms the point B_{INST_EXP} is not readily observable experimentally because of the difficulty in controlling the failure process of a unidirectional carbon fibre composite. For this reason the point I denoted as the Start of the INSTability point coming from the simulated loading curve more realistically marks the end of the experimental loading curve and of the failure of the structure. It is also experimentally possible to observe damage in the composite at this latter point, as has been shown by Scott [51].

In the case of monotonic loading followed by sustained loading, a loading curve can also be defined but in another way compared to the monotonic loading until failure. The concept of failure is evidently the same, but the quantity to consider should in general be explicitly the time variable.

Exactly analogous cases as described above but specifically for a pressure vessel are shown in (Fig. 9).

6.3. Notations for the anisotropic behaviour of the composite

For the case of a continuum consisting of isotropic linearly elastic material, even if inhomogeneous, the data for the point M consist of two coefficients (Young's modulus and Poisson's ratio) which, in a continuous framework, are sufficient for a complete definition of the behaviour and Finite Element calculations of the structure. These two coefficients allow the construction, at point M, of the 4th-order tensor linear elastic behaviour (rigidity or flexibility), noted as $\underline{c}(M)$ for

which the expression is identical in all frameworks obtained within an orthogonal transformation: the 4th-order tensor of the isotropic linear elastic behaviour of a isotropic linear elastic material is invariant for changes of ortho-normal bases. The dependence with respect to M in $\underline{c}(M)$ indicates that the continuum consists of inhomogeneous material.

In the case considered here the material making up the continuum is inhomogeneous at the macroscopic scale as it is made up of fibre volume fractions which differ at each point, $\mathcal{V}(M) = V_f(M)$. Thus the 4th-order tensor of the linear elastic behaviour (rigidity or flexibility) of the material including the dependence of the fibre volume fraction can be noted as $\underline{c}(\mathcal{V}(M))$. However the material is also anisotropic. The anisotropic framework of the material is noted as $R_{loc} = (O_{loc}, b_{loc})$, O_{loc} its origin and $b_{loc} = (\vec{x_1}^{loc}, \vec{x_2}^{loc}, \vec{x_3}^{loc})$ its base. Here we take $R_{loc} = R_y$, the framework at the microscopic scale. Thus the combined data of $\underline{c}(\mathcal{V}(M))$ and R_{loc} define the linear elastic behaviour of the anisotropic material making up the continuum of which the structure is made, describing its rigidity or its flexibility in a 4th-order tensor noted as $\underline{c}^{loc}(\mathcal{V}(M))$ ($\underline{C}^{loc}(\mathcal{V}(M))$ for the rigidity and $\underline{S}^{loc}(\mathcal{V}(M))$ for the flexibility). However, $\underline{c}^{loc}(\mathcal{V}(M))$ is not sufficient for the Finite Element calculation to be carried out. This is because the anisotropic framework has no reason to coincide with the macroscopic framework R in which the calculation is carried out (in the sense of a framework of projection) because of the arrangement of the fibres in the structure at a point M. In mathematical terms this means that the components of $\underline{c}^{loc}(\mathcal{V}(M))$ in R_{loc} have no reason to be equal to the components of $\underline{c}^{loc}(M)$ in R at point M, as in general, $R_{loc} \neq R$. Also, in addition to $\underline{c}^{loc}(\mathcal{V}(M))$, the 3 angles of Euler have to be given and then allowed to access to the local positioning of R_{loc} at each point M of the structure with respect to the R framework. Symbolically it can be noted that $R_{loc}(M)$ represents all these data. Finally, it becomes possible to calculate the components $\underline{c}^{loc}(\mathcal{V}(M))$ in the framework of projection where the calculation is made, that is R. This calculation takes place knowing $R_{loc}(M)$ and the usual formulae for the change of base for a 4th-order tensor. We can then write $\underline{c}^{ref}(M, \mathcal{V}(M))$ the 4th-order tensor (rigidity or flexibility) of the anisotropic linear elastic behaviour in M, expressed in the R framework: $\underline{C}^{ref}(M, \mathcal{V}(M))$ for the rigidity and $\underline{S}^{ref}(M, \mathcal{V}(M))$ for the flexibility.

Up to this point, we have omitted that the above reasoning does take into account the damage that can appear and be different at each M point which modifies the components of the previous 4th-order tensors. To take account of this we can write: $\underline{c}^{loc}(\mathcal{V}(M), \mathcal{D}(M,t))$, $\underline{C}^{loc}(\mathcal{V}(M), \mathcal{D}(M,t))$, $\underline{S}^{loc}(\mathcal{V}(M), \mathcal{D}(M,t))$, $\underline{c}^{ref}(\mathcal{V}(M), \mathcal{D}(M,t))$, $\underline{C}^{ref}(\mathcal{V}(M), \mathcal{D}(M,t))$ and $\underline{S}^{ref}(\mathcal{V}(M), \mathcal{D}(M,t))$.

7. A first approach to resolve the multi-scale process by a FE^2 method and orders of magnitude of length of time of the calculations. Justification of the simplified FE^2 approach

7.1. Details of the steps in the FE^2 multi-scale process

The intellectual steps for carrying out numerical calculations on real composite structures will be outlined in this section. At this stage it must be understood that the large number of very fine fibres making up the structure compared to the characteristic length of an industrial composite structure poses great difficulties in doing so in a reasonable time. The means to shorten calculation times will be explained below but here will be outlined necessary steps to be tackled even if at this stage they cannot give a final solution for the problem.

The Finite Element technique is the numerical approach used for solving the calculations. The first input data is the discretisation of the structure. In this way the number of degrees of freedom N_{ddl}, the number of elements N_{elem} and the number of Gauss Points N_{Gauss} are known. The Gauss Points are the essential points for the calculation: they play the role of the point M point in the model of the continuum. They are denoted here as M_{Gauss}. The number of degrees of freedom defines the size of the linear system to be solved during the iterations for convergence at each step of the calculation at the macroscopic level. The number of Gauss Points defines the number of times that the localisation step and that of homogenisation, for each iteration of each increment of the calculation have to be carried out at the macroscopic scale.

The different steps in the calculation explained (Section 6.2.1) are as follows:

- Step 0 - Execution of Monte-Carlo processes which affect the values (these will be discussed later and their number defined) of strengths of fibres at each Gauss Point and also the local fibre volume fraction at each Gauss Point;
- Step I - I-th time increment. The change in load or not on the structure (the latter in the case of a steady load for example);
- Step RMi - Resolution to convergence of the I-th time increment at the macroscopic scale so as to obtain the macroscopic stress and strain fields at each of the N_{Gauss} Gauss Points. So as to arrive at convergence, N_{RMi} iterations are necessary. At each of these iterations at each Gauss Point M_{Gauss}:
    - . Step LM_{Gauss} - Localisation step - This is a Finite Element calculation on the RVE characteristics of the Gauss Point which allows the stress and strain fields to be known

in all the RVE which then permits an increase in the number of fibres which break (Eq. 4);

. Step HM_{Gauss} - Homogenisation step - This is carried out using Finite Elements to resolve six elementary problems (loading of the RVE with the six usual symmetrical 2-tensor base) on the RVE characteristic of the Gauss Point, followed by averaging on the six solutions. This step gives $\underline{\underline{C}}^{loc}(\mathcal{V}(M),\mathcal{D}(M,t))$, $\underline{\underline{S}}^{loc}(\mathcal{V}(M),\mathcal{D}(M,t))$ then $\underline{\underline{C}}^{ref}(\mathcal{V}(M),\mathcal{D}(M,t))$, $\underline{\underline{S}}^{ref}(\mathcal{V}(M),\mathcal{D}(M,t))$, used for the calculation of the macroscopic scale;

- Step Failure - The condition of the structure is examined to determine if failure has happened at the end of the I-th step in the calculation (when convergence has occurred). If failure has occurred the calculation is stopped but if not the time-loading step is increased (Step I).

7.2. A simple example allowing the calculation time to be evaluated showing that the technique cannot give a solution

Consider a pressure vessel which is made by filament winding carbon fibres over a mandrel which becomes the liner. Locally the fibres are arranged in a unidirectional manner and are subjected only to tensile loads when the vessel is pressurised as they are automatically placed on geodesic paths during manufacture. Consider such a pressure vessel for which its internal length is 700 mm and internal diameter is 100 mm. It is supposed that the wall of the composite has a fibre volume fraction of 64%. As above it is taken that the composite assures the mechanical strengths of the pressure vessel and that the fibres can fail in the same manner as in a unidirectional composite.

If only the cylindrical part of the pressure vessel, of length 500 mm, is considered with a discretisation at the macroscopic scale with elements having approximately the dimensions of eight RVE (0.1 mm $\times$ 0.1 mm $\times$ 8.0 mm, Section 5), this part of the composite structure contains about 400000 hexahedral elements each having eight nodes and eight Gauss Points giving 800000 degrees of freedom and 3200000 Gauss Points at the macroscopic scale. It can be estimated then that iteration in the Finite Element calculation at the macroscopic scale involving the inversion of a linear system containing 800000 unknowns would last approximately 60 seconds with a standard configuration computer. Furthermore, so as to carry out the localisation and homogenisation (once more with the Finite Element technique, which explains the name FE^2), the multi-scale process needs the dicretisation of the RVE at the microscopic scale. For a sufficiently fine dicretisation to be carried out so as to model fibre failure it would involve 250000 degrees of freedom. The steps of localisation and homogenisation require, as mentioned above, the resolution of 1+6 problems,

which by the Finite Element technique means seven inversions of a linear system with 250000 unknowns and of the average operations: that is estimated to take ten seconds.

These operations at the microscopic scale must be carried out as many times as the number of Gauss Points, which means that one iteration in one increment of the multi-scale calculation takes 32 million seconds (rather more than one year). The calculation time at the macroscopic scale ($\approx$ 60 seconds) is negligible compared to the calculation which is necessary at the microscopic scale ($\approx$ 32000000 seconds). Knowing that a single increment of the calculation made close to the failure point of the structure can require several tens of iterations to achieve convergence it is easy to understand that the complete simulation of the failure of a pressure vessel by this approach would be inaccessible to an industrial design team.

It is therefore necessary to find another solution. To achieve this we will take an analytical approach for the steps at the microscopic scale. The precise details of this approach are given in the following section. However the main outlines are as follows:

- investigate, by Finite Element analysis, a large number of microscopic configurations for the RVE which are possible to encounter during the calculation;
- store in a data base all the possible cases considered and their results.

Then, during the calculation process which conserves the resolution of the Finite Element analysis on the macroscopic scale, at each Gauss Point, the configuration of the RVE will be identified and its state found from the data base. This approach will be called the FE^2 simplified method. It will be shown that with this technique the calculation time at the microscopic scale will be drastically reduced ($\approx$ several seconds instead of 3200000 seconds) and that it becomes negligible when compared to the macroscopic step ($\approx$ 60 seconds).

Using this approach a provisional study of the pressure vessel becomes possible.

8. Creation of the simplified multi-scale FE^2 process

8.1. Resolution of the homogenisation step by an analytical approach: behaviour at the macroscopic scale, hypotheses

The first hypothesis is that the principal process governing failure of the structure is the breakage of the reinforcing continuous fibres. As a consequence of this supposition the non-linearity of the macroscopic behaviour of a unidirectional composite which occurs when the material is loaded perpendicularly to the the fibres or in shear (due to intralaminar cracking or viscoelastic behaviour)

is not considered. The second hypothesis concerns the behaviour parallel to the fibre direction. Based on experimental observations (Section 4.3), and in contrast to the microscopic scale, it is considered that any non-linearity parallel to the fibres, due to the viscoelasticity of the matrix, can be ignored. It is accepted that the non-linearity must exist but that it is negligible compared to the effects due to the failure of the fibres.

Finally, the only non-linearity visible at the macroscopic scale is that in the axis of the fibres and is due to their failure. This effect is directly due to the local density of broken fibres described with $\mathcal{D}(M,t)$, at the point M at time t. Thus, finally, in the local anisotropic framework of the material, the dependence of the behaviour on damage is revealed by writing the 4th-order tensor of the linear elastic behaviour: $\underline{\underline{C}}^{loc}(\mathcal{V}(M),\mathcal{D}(M,t))$. As has already been shown the simulation of this behaviour (resolution of problems of homogenisation) is made using a numerical route, in particular by Finite Element analysis, which can be long and costly. However, in the case considered only the component C^{loc}_{1111} from $\underline{\underline{C}}^{loc}(\mathcal{V}(M),\mathcal{D}(M,t))$ is affected by fibre failure. It can therefore be shown that due to the large differences in properties between the fibres and matrix a good approximation for the value of the component $C^{loc}_{1111}(\mathcal{V}(M),\mathcal{D}(M,t))$ is given by the classic law of mixtures analysis which gives:

$$\begin{aligned} C^{loc}_{1111}(\mathcal{V}(M),\mathcal{D}(M,t)) = V_f(M)C^f_{1111}(1-\mathcal{D}(M,t)) \\ + (1-V_f(M))C^m_{1111} \end{aligned} \tag{5}$$

with:

- $\mathcal{D}(M,t) = \frac{N_R(M,t)}{N_T}$ where $N_R(M,t)$ designates the number of broken fibres in the RVE RVE(M) at t and $N_T = 32$ the total number of fibres which is identical for all the RVE;
- C^f_{1111} and C^m_{1111} designates the component along the vector $\vec{x_1}^{loc}$ in the R_{loc} framework of the 4th-order tensor of rigidity respectively of the fibres and the resin, both seen as continuous phases at the microscopic scale. In reality as these constituents are considered isotropic for this calculation this precision is not necessary. Nevertheless it is accepted that carbon fibres are anisotropic but are transversely isotropic which is only what matters in this simulation but could be an issue in a further development;
- $V_f(M)$ designates the local fibre volume fraction in the RVE(M) and is time independent.

Finally, at the macroscopic scale and in the R framework, the anisotropic and inhomogeneous linear elastic behaviour of the material, which can be damaged so as to become non-linear, obtained from $\underline{\underline{C}}^{loc}(\mathcal{V}(M),\mathcal{D}(M,t))$ et $R_{loc}(M)$, is written as:

$$\sigma(M,t) = \underline{C}^{ref}(M, \mathcal{V}(M), \mathcal{D}(M,t))\varepsilon(M,t)$$

$$\Longleftrightarrow$$

$$\varepsilon(M,t) = \underline{S}^{ref}(M, \mathcal{V}(M), \mathcal{D}(M,t))\sigma(M,t)$$

More precisely, the access to $\underline{C}^{ref}(M, \mathcal{V}(M), \mathcal{D}(M,t))$ takes place in two steps:

- to begin with the resolution in the R_{loc} framework, of the problems of homogenisation concerning RVE(M) degraded by the failure of fibres at point M at t, which gives $\underline{C}^{loc}(\mathcal{V}(M), \mathcal{D}(M,t))$. Here it is the analytical formula (Eq. 5) which is used. The use of this formula is much less onerous than using Finite Element analysis and allows a considerable reduction in calculation time;
- then by knowing $R_{loc}(M)$ and the usual formulae for the changes of bases for a 4th-order tensor, which give $\underline{C}^{ref}(M, \mathcal{V}(M), \mathcal{D}(M,t))$.

The choice above is that it is the failure of the fibres which is by far the principal damage process. It is the only phenomenon to be considered and its impact described by $C^{loc}_{1111}(\mathcal{V}(M), \mathcal{D}(M,t))$, justifies totally that only the axial stress supported by the fibres F_i, $s^{F_i}_{11}(P,t)$, is finally important in the failure process of the structure. It is therefore the reason why our interest will be concentrated on it at the microscopic level and notably on the increase in load on the remaining intact neighbouring fibres which can break when the matrix relaxes. So as to reinforce the importance of this effect it should be remembered that it is this stress averaged on the the cross-section $S_{F_i}(y_1)$ placed on the abscissas y_1, $\langle s^{F_i}_{11}(P,t)\rangle(y_1,t)$, which causes, or not, the failure of the fibre F_i.

8.2. Preparation for the resolution of the localisation step by an analytic process. Modelling of the phenomenon of fibre failure at the microscopic scale

Following from what has been described above it becomes clear that the phenomenon which must be understood is the transfer of axial loads between neighbouring fibres within a RVE representing a given fibre volume fraction:

- when fibres break;
- when the failure of fibres induces debonding from the matrix at the point of the break;
- when, in addition to the previous phenomena the matrix is considered to be viscoelastic and so leads, as a function of time, to a transfer of load from the broken fibre to its neighbours an increase in load which evolves with time.

8.2.1. Hypotheses concerning the failure of fibres at the microscopic scale. Notions of i-plets

The bidimensional work of Baxevanakis [38] (confirmed by those of Rojek [54] for thee dimensionnal case) showed that the state of failure of the RVE, on average, had the following characteristics:

- the fibres are broken once in the RVE;
- the breaks are in the same plane within the RVE.

For the sake of this simulation the fibres are considered to be organised as a square array (Section 5). In the same way it will be supposed that the fibre breaks respect a regular periodicity in the geometry of the RVE. In this way it is assumed that the passage from an intact (no broken fibres in the RVE) described by the RVE noted as $CS32$ (Fig. 10), to a material totally degraded in which all the fibres of the RVE are broken in the same plane, noted as the RVE described as $C1$. (Fig. 10) goes through five distinct states of damage in which the RVE contains 1, 2, 4, 8 and 16 broken fibres. The RVE representing the different states of damage are respectively $C32, C16, C8, C4, C2, C1$ (Fig. 10) and define i-plets representing the numbers of broken fibres (i broken fibres in a RVE): $C32$ defines 1-plet (1 broken fibre of the original 32), $C16$ defines a 2-plet (2 broken fibres of the 32), $C8$ defines a 4-plet (4 broken fibres of the 32), $C4$ defines a 8-plet (8 broken fibres of the 32), $C2$ defines a 16-plet (16 broken fibres of the 32), $C1$ defines a 32-plet (all 32 fibres are broken). The RVE $CS32$ defines therefore a 0-plet which is characteristic of the undamaged state of the composite.

8.2.2. The load transfer coefficient

The longitudinal coefficient of load transfer [15] [16] [17] [18], noted as k_r, is defined for:

- a fibre volume fraction V_f;
- a damage state represented by the RVE C ($C = CS32$, $C32$, $C16$, $C8$, $C4$, $C2$, $C1$);
- a fibre F_i ($i = 1, \ldots, 32$);
- a debonding length d;
- the time t;
- a value Y_1 of the coordinate y_1 along the fibre axis measured from the plane of fibre failure,($y_1 = 0$),

by:

$$k_r\left(V_f, C, F_i, d, t, Y_1\right) = \frac{\int_{Y_{1j}}^{Y_{1j+1}} \left(\int_{S_{F_i}(y_1)} s_{11}^{F_i}\left(V_f, C, d | y_1, y_2, y_3, t\right) dy_2 dy_3 \right) dy_1}{\int_{Y_{1j}}^{Y_{1j+1}} \left(\int_{S_{F_i}(y_1)} s_{11}^{F_i}\left(V_f, CS32, d = 0 | y_1, y_2, y_3, t = 0\right) dy_2 dy_3 \right) dy_1} \tag{6}$$

where:

- y_2, y_3 designates the coordinates identifying the cross-section of the fibre;
- Y_{1j} et Y_{1j+1} are the axes of the cross-sections between which are calculated the coefficient k_r;
- $Y_1 = \frac{Y_{1j+1}+Y_{1j}}{2}$;
- $S_{F_i}(y_1)$ designates the cross-section of the fibre F_i considered, in y_1. Here, it should be recalled that given the hypothesis (Section 5), $S_{F_i}(y_1) = S_F$;
- $s_{11}^{F_i}\left(V_f, C, F_i, d | y_1, y_2, y_3, t\right)$ is the axial stress $s_{11}^{F_i}(y_1, y_2, y_3, t)$ in the fibre F_i for the case where the fibre volume fraction is equal to V_f, of the damage state RVE C for a debonding length of d.

It is considered that the relationships between failure, debonding and relaxation of the matrix are of second order in importance. Also so as to separate their effects on the load transfer we write:

$$\begin{aligned} k_r\left(V_f, C, F_i, d, t, Y_1\right) = & 1 + \\ & K_r\left(V_f, C, F_i, d = 0, t = 0, Y_1\right) + \\ & K_d\left(V_f, C, F_i, d, t = 0, Y_1\right) + \\ & K_v\left(V_f, C, F_i, d = 0, t, Y_1\right) \end{aligned} \tag{7}$$

and the following are calculated separately:

- $K_r\left(V_f, C, F_i, d = 0, t = 0, Y_1\right)$ which is the part of the load transfer exclusively due to the fibre breaks;
- $K_d\left(V_f, C, F_i, d, t = 0, Y_1\right)$ which is the part due to the load transfer associated with the length of debonding. This length varies between 0 and 35 μm from the plane of the fibre break. The value of 35 μm has been determined experimentally and results in a maximum of local transfert to neighboring intact fibres;
- $K_v\left(V_f, C, F_i, d = 0, t, Y_1\right)$ is due to the load transfer due to the relaxation of the matrix.

8.2.3. The most unfavourable value of the load transfer coefficient. Construction of a data base for the localisation step

For safety considerations a conservative evaluation of failure is considered by using the most unfavourable value of the load transfer coefficient. This means that the maximum values of the above functions will be considered, so that:

$$\begin{aligned} k_r^{MAX}(V_f, C, t) = & 1 + \\ & K_r^{MAX}(V_f, C) + \\ & K_d^{MAX}(V_f, C) + \\ & K_v^{MAX}(V_f, C, t) \end{aligned} \tag{8}$$

with:

$$\begin{cases} K_r^{MAX}(V_f, C) = \max\limits_{F_i, Y_1} K_r(V_f, C, F_i, d = 0, t = 0, Y_1) \\ K_d^{MAX}(V_f, C) = \max\limits_{F_i, Y_1, d} K_d(V_f, C, F_i, d, t = 0, Y_1) \\ K_v^{MAX}(V_f, C, t) = \max\limits_{F_i, Y_1} K_v(V_f, C, F_i, d = 0, t, Y_1) \end{cases} \tag{9}$$

Smoothing is carried out of the calculated points obtained above by simple polynomials. During the multi-scale process the value V_f and C lead directly to the value of the maximum transferred load transfer in an analytical form and not as a Finite Element result.

8.2.4. Evolution of the fibre break phenomenon at the microscopic scale during the simplified FE^2 multi-scale process

The evolution of the fibre breaks is governed, in the most general case, by the condition (Eq. 4, Section 6.2.1). However, taking into account the preceding section (Section 8.2.1), at the level of the RVE in the simplified process FE^2 the evolution of the process can be evaluated as follows:

- at each point M_{Gauss}, for a fibre volume fraction of V_f, at each RVE with characteristics of the damage states which are likely to be met, C ($C = CS32, C32, C16, C8, C4, C2$) is associated a failure value noted as $s_R^F(V_f, C)$ from the Monte-Carlo process given in the step 0 (Section 7.1) which assigns six values to each Gauss Point;
- if the value is known for M_{Gauss}:
  - . the loading (which is to say the macroscopic stress M applied to the RVE RVE(M_{Gauss});
  - . the local fibre volume fraction V_f (Step 0, Section 7.1);
  - . the actual damage state of RVE(M_{Gauss}) characterised by RVE C;

. the time t;

the data base $k_r^{MAX}\,(V_f, C, t)$ supplies the value of the maximum stress in the fibres within the RVE (M_{Gauss}), noted as $s^F_{MAX}(V_f, C, t)$;

- to make evolve the process of fibre breakage in M_{Gauss}, the following condition has to be evaluated:

$$s^F_{MAX}(V_f, C, t) \geq s^F_R(V_f, C)? \tag{10}$$

If the condition is not verified nothing happens. If it is verified the fibre breaks at M_{Gauss} evolve:

. if $C = CS32$, so one fibre breaks and the state of the RVE $CS32$ evolves to $C32$;

. if $C = C32$, then one more fibre breaks and the state of the RVE $C32$ evolves to $C16$;

. if $C = C16$, then two further fibres break and the state of damage of the RVE $C16$ evolves to $C8$;

. if $C = 8$, then for more fibres break and the the state of damage of the RVE $C8$ evolves to $C4$;

. if $C = 4$, then eight more fibres break et the state of damage of the RVE $C4$ evolves to $C2$;

. if $C = 2$, then sixteen more fibres break and the state of damage of the RVE evolves to $C1$.

9. Applying the approach: calculating the response of the composite structure until failure. Description of the general functioning framework

9.1. General considerations and hypotheses

All the material systems studied are being displaced in the physical space ε^3 with respect to the framework $R = (O, b)$ (macroscopic scale), supposed to be Galilean, for which the base is $b = (\vec{x}_1, \vec{x}_2, \vec{x}_3)$ and O the origin. They are all, or in part, composed of unidirectional composite material composed of fibres and resin (carbon fibres and epoxy resin to be precise unless otherwise stated) of which can be noted $b_{loc} = (\vec{x_1}^{loc}, \vec{x_2}^{loc}, \vec{x_3}^{loc})$ the base of the local anisotropy framework $R_{loc} = (O_{loc}, b_{loc})$ for which the vector $\vec{x_1}^{loc}$ is aligned with the fibre axis (local anisotropy framework, Section 6.3). For the parts of the structure made of composite material, $R_{loc}(M)$ designates the position of R_{loc} at the point M, knowing, for example, the Euler angles at the point M which allow to bring $R_{loc} = R$ (by definition of Euler's angles) on $R_{loc}(M)$ (Section 6.3).

Concerning the failure strength of fibre $\mathcal{P}^R(M)$ are given in each point of the structure. Numerically, a Monte-Carlo process attributes six values at each Gauss Point of the structure. These values are necessary to enable the kinetics of fibre failure to be included in the simulation (Section 8.2.4).

The initial state of the considered structure regarding the damage is the following: the material is free of fibre break at each point. Then $\mathcal{D}(M,t)) = 0$ for all point.

The initial state of the considered structure regarding the local volume fraction could be the following: a local fibre volume fraction presenting a random characteristic but supposed constant as a function of time. In this case, numerically, a Monte-Carlo process attributes a local fibre volume fraction to each Gauss Point of the structure. But in the following applications the random fibre volume fraction will not be considered. Then at all points in the structure the local volume fraction is considered identical and constant over time.

We shall consider the following hypotheses:

- small displacements;
- at all times the system is supposed to be in a quasi-static equilibrium;
- Gravity effects are neglected;
- it is supposed that there are negligible variations in temperature due to dissipation processes, particularly the failure of fibres. The temperature of the system is therefore uniform and constant with time;
- the behaviour of the material considered is, for the given damage state, anisotropic linear elastic.

9.2. Formulation of the most general problem. Resolution at the macroscopic scale

The material system S studied is being displaced and coincides in time with the domaine $D = \Omega \cup \partial\Omega$. D is a continuous path-connected bounded and closed set in ε^3, Ω designates its interior and $\partial\Omega$ its boundary which is considered to be regular. More precisely, D coincides with $D(t) = \Omega(t) \cup \partial\Omega(t)$ at time t and with $D_0 = D(t_0) = \Omega(t_0) \cup \partial\Omega(t_0)$ at time t_0. At time t, the outer unit vector in a point M of $\partial\Omega$ is noted as $\vec{n}(M,t)$.

The evolution of the domain is studied between times t_0 and t_{max}.

The loadings applied to the domain can be: remote actions acting on $\Omega(t)$ and induced by a volume density of force denoted $\rho(M)\vec{f}(M,t)$ (induced by Gravity for example) and contact actions on $\partial\Omega(t)$. Here the hypotheses assume that the effect of gravity is negligible with respect to other loads. Thus: $\rho(M)\vec{f}(M,t) = \vec{0}$.

To construct a general framework for the contact actions it is necessary to divide the frontier of the domain into three distinct parts $\partial\Omega_U$, $\partial\Omega_F$ and $\partial\Omega_{FU}$. It is supposed that this division is independent of time and that it forms a partition of $\partial\Omega(t)$, which is to say that summing the different parts reforms the totality of $\partial\Omega(t)$ and that their intersection two by two is equal to the empty set:

$$\partial\Omega(t) = \partial\Omega_U \cup \partial\Omega_F \cup \partial\Omega_{FU} \qquad \left\{ \begin{array}{l} \partial\Omega_U \cap \partial\Omega_F = \emptyset \\ \partial\Omega_F \cap \partial\Omega_{FU} = \emptyset \\ \partial\Omega_U \cap \partial\Omega_{FU} = \emptyset \end{array} \right.$$

One or two of these parts can be equal to the empty set. However, when a part is not equal to the empty set, it is imposed that its measure (its area) is strictly positive. Starting from this division, we define the following general boundary conditions:

- on $\partial\Omega_F$, the surface density of force $\vec{F}(M,t)$ is given;
- on $\partial\Omega_U$, the displacement field $\vec{U}(M,t)$ is given;
- on $\partial\Omega_{FU}$, a local vector of information, for which one component can be a component of a surface density of force or a component of a displacement field, is given. For instance:

$$\left(\begin{array}{c} F'_1(M,t) \\ U'_2(M,t) \\ F'_3(M,t) \end{array} \right)$$

where $F'_1(M,t)$ and $F'_3(M,t)$ are the first and third components of a surface density of force $\vec{F}'(M,t)$ and $U'_2(M,t)$ the second component of a displacement field $\vec{U}'(M,t)$.

These boundary conditions are those of a so-called standard problem. Associated with linear elastic behaviour (as considered here, for a given damage state) they are those of a standard problem of linear elasticity (given in the following section). In this case, theorems exist that give the existence and uniqueness of the solutions of this problem.

The problem which has to be solved consists of finding, at each M point of the domain the following unknowns:

- the displacement vector $\vec{u}(M,t)$;
- the stress tensor $\sigma(M,t)$;
- the damage variable $\mathcal{D}(M,t)$ relative to the number of broken fibres in M at t, $N_R(M,t)$,

verifying:

- the local equation of equilibrium (including the hypotheses given):

$$\overrightarrow{div}\,\sigma(M,t) = \vec{0}\ \forall M \in \Omega(t)$$

- the behaviour law
  - . state law: $\sigma(M,t) = \underline{C}^{ref}(M,\mathcal{D}(M,t))\varepsilon(\vec{u}(M,t)) \Longleftrightarrow \varepsilon(\vec{u}(M,t)) = \underline{S}^{ref}(M,\mathcal{D}(M,t))\sigma(M,t)$;
  - . evolution law of the fibre failure at point M: knowing $\sigma(M,t)$, $V_f(M)$ and $\mathcal{D}(M,t)$ (therefore the RVE characteristic C) and $t \Rightarrow$ analytical localisation step in the simplified multi-scale calculation and fibre break evolution (Section 8.2)
    - * consultation of the database (Section 8.2.3) giving $k_r^{MAX}(V_f,C,t) \Rightarrow$ access to the maximum axial stress $s^F_{MAX}(V_f,C,t)$ in the fibres of RVE C
    - * knowing the value of the failure stress of fibres (Monte-Carlo process at the beginning of the calculation) likely to cause further fibre breaks, $s^F_R(V_f,C)$
    - * examine the condition $s^F_{MAX}(V_f,C,t) \geq s^F_R(V_f,C)$ (Section 8.2.4) ?
    - * if the condition is verified the damage state will increase.Then the mechanical properties of the new state of the material can be calculated at M ($\Rightarrow$ analytical homogenisation step of the simplified multi-scale process, Section 8.1)
    - * if the condition is not verified the damage state remains the same
- boundary conditions:

$$\begin{cases} \text{on } \partial\Omega_F \ : \ \sigma(M \in \partial\Omega_F,t) \times \vec{n}(M \in \partial\Omega_F,t) = \vec{F}(M,t) \\ \text{on } \partial\Omega_U \ : \ \vec{u}(M \in \partial\Omega_U F,t) = \vec{U}(M,t) \\ \text{on } \partial\Omega_{FU} \ : \begin{cases} \{\sigma(M \in \partial\Omega_{FU},t) \times \vec{n}(M \in \partial\Omega_{FU},t)\}_1 = F'_1(M,t) \\ \{\vec{u}(M \in \partial\Omega_{FU},t)\}_2 = U'_2(M,t) \\ \{\sigma(M \in \partial\Omega_{FU},t) \times \vec{n}(M \in \partial\Omega_{FU},t)\}_3 = F'_3(M,t) \end{cases} \end{cases}$$

10. Applying the approach: calculating the response of a simple composite structure until failure. Case of a parallelepiped specimen

10.1. Description of the structure and loading conditions

The purpose of this section is show how the model described in earlier sections of the paper can be applied to structures. Initially a simple structure will be described under two types of load and the kinetics of damage accumulation calculated in each case. This will lead to applying the model to an industrial pressure vessel under analogous loading conditions which however relate to real conditions experienced by pressure vessels. In each case the mechanisms of damage accumulation will be compared as a function of the loading conditions.The initial system studied S is a parallelepiped specimen reinforced parallel to its major axis. The specimen considered is taken to be a composite plate delimited by the following surfaces:

- S_{-a} situated at $x_1 = -a$ and S_{+a} situated at $x_1 = +a$;
- S_{-b} situated at $x_2 = -b$ and S_{+b} situated at $x_2 = +b$;
- S_{-c} situated at $x_3 = -c$ and S_{+c} situated at $x_3 = +c$.

The long axis of the specimen is described by the vector $\vec{x_1}$. The width is oriented by the vector $\vec{x_2}$ and the thickness by the vector $\vec{x_3}$. The plane of the specimen is defined by the vectors $\vec{x_1}$ and $\vec{x_2}$. The cross section of the specimen is therefore defined by the vectors $\vec{x_2}$ and $\vec{x_3}$. For the simulation the dimensions are $2a = 40$ mm, $2b = 4$ mm, $2c = 1$ mm. The specimen is made up of a unidirectional composite at 0°,which is to say that at every point of the structure $R_{loc}(M) = R$.

The boundary conditions are taken to be the following (with $F_s(t) \geq 0$):

- on S_{-a}, a uniform surface density of force is applied $\vec{F}_{-a}(M,t) = -F_s(t)\vec{x_1}$;
- on S_{+a}, a uniform surface density of force is applied $\vec{F}_{+a}(M,t) = +F_s(t)\vec{x_1}$;
- the other surfaces are free of force;
- giving $\partial\Omega_F = \partial\Omega(t)$, $\partial\Omega_U = \emptyset$, $\partial\Omega_{FU} = \emptyset$.

Two types of loadings are considered:

- monotonic loadings increasing until failure, called ML (Monotonic Loading): the effect of loading rate on failure strength of the structure is studied. Two loading rates are considered: 0.02 MPa/s and 20 MPa/s and are called $ML002$ and $ML20$. Only one Monte-Carlo run, denoted as $MCR001$, has been considered here for each calculation. To clearly see the rate

effect the same Monte-Carlo run has been used for these two calculations. The value of the load at the SINST Point for each calculation, for this Monte-Carlo run $MCR001$, is noted respectively $F^{MCR001}_{SINST\_002}$ and $F^{MCR001}_{SINST\_20}$;

- increasing monotonic loadings which are stopped before failure of the composite and held steady until delayed failure occurs, called here SL (Sustained Loading). Here, the load is increased until $0.90 \times F^{MCR001}_{SINST\_20}$ at 20 MPa/s then sustained. The point noted as SSL Point (Start of the Sustained Loading) defines the point where the loading is maintained constant. Here also only one Monte-Carlo run has been considered, the same $MCR001$ as for the previous case. The objective here is to point out that the clustering effect is completely different in the ML and SL cases.

For the ML cases, the loading curve (Section 6.2.2) is defined by $F =< \sigma_{11} >$ function of $U =< \varepsilon_{11} >$. For the SL case, the loading curve is defined by $< \varepsilon_{11} > / < \varepsilon_{11} >_{SSL}$ function of t/t_{SSL}.

10.2. Results of the calculations

The results and analysis are made on the loading curves and the populations of 0-plets and 32-plets (Fig. 11 for ML case, Fig. 12 for SL case).

Figure 11 shows clearly the effect of speed of loading. The reduced rate of loading allows the viscoelastic nature of the matrix to increase damage so that the critical point in loading is reduced, resulting in a decrease in breaking load. There is no attempt here to include an affect which is also induced by the viscoelastic behaviour of the matrix which is to allow straightening of the fibres under the loads which they are supporting. This is known to increase the strength of carbon fibre composites and can lead to an increase in strength of a structure after prolonged steady loading or cyclic loading. The effects of increasing fibre breaks and straightening of the fibres are in competition but while the latter effect is expected to slow and cease the former progressively increases damage. Equally there is no attempt to include other mechanisms seen with other reinforcements such as glass fibres which suffer from stress corrosion or creep seen with aramid fibres. There are no reasons why these effects could not be added to the simulation if required. The plateaux shown in the curves are a consequence of the type of calculation carried out and should not be considered to represent what happens in reality although they are analogous to those described in the most general model of composite behaviour described by Aveston, Cooper and Kelly [56] [57].

The effects of loading a composite plate are illustrated in (Fig. 11) and are increasing numbers of fibre breaks leading to the formation of groups of breaks. These are described as i-plets where

i indicates the number of breaks in a cluster. Initial damage in the composite is similar to that seen in a fibre bundle. That is to say that individual fibres break at their weakest points and these points of failure are both unrelated to each other and are randomly arranged in the composite. Nevertheless chance will play a part in this process so that neighbouring fibres could break in the same plane and this may even be encouraged by contacts between fibres. Increasing numbers of small groups of breaks lead to a concentration of local stresses with multiple associated breaks occurring producing an increasingly unstable situation, although no overall change in composite behaviour will be observed. This is because the breaks are isolated in the composite by shearing of the matrix around the breaks and have an insignificant effect on the overall behaviour. Figure 11 shows the most dramatic situation for loading at 0.02 MPa/s where all the fibres in the RVE break. This is the 32-plet case. It can be seen that this situation occurs just before complete failure and clearly is its cause. Significantly the changes in the numbers of 0-plets show that even just before the point of failure about 75% of all the fibres in the composite are unbroken. The model allows the effects of loading speed to be examined. Figure 11 shows results at a loading speed of 20 MPa/s and shows that as the higher speed failure occurs more rapidly when 32-plets develop. Again most fibres in the composite are undamaged just before this sudden death failure of the composite.

A comparison between the monotonic loading case described above and the effects of steady loading, as shown in Figure 3 obtained from experiments, is revealing. The model explains how it is the viscoelastic nature of the matrix which determines damage accumulation in the form of fibre breaks when the composite is subjected to stress particularly over long times. Figure 12 shows an simulated curve for a unidirectional carbon fibre composite loaded to very near its expected tensile breaking load. Damage in the specimen shown in Figure 3 was monitored using acoustic emission and the curve of damage as a function of time is exactly similar to that obtained at lower loads and importantly, as will be further explained in the next section, to that obtained when a carbon fibre pressure vessel is held at a constant pressure or cycled up to a given pressure. The advantage of loading to near the failure load was that results could be obtained in just a few hours and as will be explained loading at lower loads leads to much greater scatter in lifetimes making experiments costly in time and money if applied to pressure vessels. Figure 12 shows that during the steady loading damage increases at a decreasing rate but does not stop. Eventually the curve of damage against time increases rapidly and failure occurs. Figure 12 shows that the model described above based on the physical processes observed in composite failure describes well the behaviour shown in (Fig. 3). Modelling of damage accumulation in a composite structure

such as a carbon fibre composite pressure vessel allows the kinetics of damage accumulation to be determined for very long periods of test. If a structure is subjected to a constant load, necessarily lower than its breaking load as determined by monotonic loading, it will be able to sustain greater damage without breaking than that at a higher load.

11. Applying the approach: calculating the response of a high pressure composite vessel. Statistical aspects of the burst and intrinsic safety factor

11.1. Objectives

The effects of long term loading on advanced composite structures is now a major interest as they are now being used for major critical civil applications. This is nowhere more evident than for the use of carbon fibre composite pressure vessels which will enable the forthcoming hydrogen economy to be realised. Hydrogen will be and is at present being stored in these vessels, typically at a pressure of 70 MPa that is to say 700 atmospheres. This is a very high pressure and certainly the smallest risk of failure has to be avoided. There is an urgent need for a quantitative understanding of damage processes in these structures and as explained earlier present proof tests are misconceived. The result is that composite pressure vessels today are over designed so as to avoid failure and with very few exceptions this has been successful in avoiding accidents however it is clearly necessary to design structures such as composite pressure vessels based on a quantifiable knowledge of damage kinetics for use over periods of decades. One significant advantage would be economic as by far the greatest part of the costs of producing carbon fibre pressure vessels is the purchasing of the fibres. The above model allows such a quantifiable understanding of the damage kinetics when a carbon fibre composite pressure vessel is either pressurised monotonically to burst or is subjected to use under high pressure for prolonged periods of perhaps decades. Of course the above analysis considers only the intrinsic nature of damage in a composite structure and not effects such as human error during manufacture or external damage which might occur but for the first time it allows damage to be quantified within such an advanced composite structure.

The following section applies the lessons learned from the preceding calculation of loading a composite plate to a filament wound pressure vessel for which both the effects of monotonic pressurisation to failure and constant pressure held over long periods will be examined. The questions to which we want to find an answer are, in particular:

- in the case of rapid monotonic increasing pressure applied to vessels, how large is the scatter in the burst pressure of the vessels?

- in the case of sustained pressure applied to vessels, how large is the scatter in the time-to-failure of the vessels?

- in the case of sustained pressure applied to vessels, does the scatter in the time-to-failure depend on the level of the sustained pressure?

11.2. Description of the structure and loading conditions

For confidential reasons, description, calculations and results made on real industrial pressure vessels cannot be presented. Then, here, the material system to be studied S is a small but representative pressure vessel. However, this does not affect significantly, the methodology, the process and results, except concerning the duration of calculations.

Then, here the material system to be studied S consists of a central cylindrical part C of length L enclosed at each end by two hemispherical domes H_- and H_+ with centres O_- and O_+ (Fig. 14). In the observation framework R, the main axis of the pressure vessel is orientated by the vector $\vec{x_3}$ and $\overrightarrow{OO_-} = -\frac{L}{2}\vec{x_3}$, $\overrightarrow{OO_+} = \frac{L}{2}\vec{x_3}$. It can be noted respectively that S_{int} and S_{ext} define the internal and external surfaces of the vessel. They are characterised by the radii r_{int} and r_{ext} and the total wall thickness of the pressure vessel is e. The pressure vessel consists of a liner of thickness e_l and a composite wrapping produced by filament winding. The stratified composite wrapping covering the liner is described by the winding angles as $(90°, +20°, -20°)$ (from the outer to the inner of the vessel) such that:

- in the cylindrical part,

$$\begin{aligned} b_{loc}(M) &= (\vec{x_1}^{loc}(M), \vec{x_2}^{loc}(M), \vec{x_3}^{loc}(M)) \\ &= (\vec{e_\varphi}(M), \vec{x_3}(M), \vec{e_l}(M)) \end{aligned}$$

  where the vectors $\vec{e_l}(M)$, $\vec{e_\varphi}(M)$, $\vec{x_3}(M)$ are those of the usual local framework at M defined by cylindrical coordinates (l, φ, x_3);

- in the hemispherical domes,

$$\begin{aligned} b_{loc}(M) &= (\vec{x_1}^{loc}(M), \vec{x_2}^{loc}(M), \vec{x_3}^{loc}(M)) \\ &= (\vec{e_\theta}(M), \vec{e_\varphi}(M), \vec{e_r}(M)) \end{aligned}$$

  where the vectors $\vec{e_r}(M)$, $\vec{e_\theta}(M)$, $\vec{e_\varphi}(M)$ are those of the usual local framework at M defined by spherical coordinates (r, θ, φ) of which the centres are respectively O_- and O_+.

The dimensions chosen are: $L = 10$ mm, $r_{int} = 7$ mm , $r_{ext} = 8.20$ mm, $e = 1.20$ mm, $e_l = 0.2$ mm. The thickness of the composite is therefore 1 mm distributed in the following manner: first ply 1 at 90° with a thickness of 0.4 mm, second ply 2 at +20° with a thickness of 0.3 mm, third ply 3 at −20° with a thickness of 0.3 mm. The liner is considered to be made of aluminium.

The following boundary conditions are used:

- a uniform pressure p_{int} having a value $P(t) \geq 0$ applied to the surface S_{int} giving a surface density of force $\vec{F}_{int}(M,t) = -P(t)\vec{n}(M,t)$;
- a uniform zero pressure p_{ext} was applied to the surface S_{ext} giving a surface density of force $\vec{F}_{ext}(M,t) = \vec{0}$ (surface free of force);
- giving $\partial\Omega_F = \partial\Omega(t)$, $\partial\Omega_U = \emptyset$, $\partial\Omega_{FU} = \emptyset$.

A first analysis is made and the intention is to observe the effect of the pressurisation rate on the burst pressure. To do so Monotonic Increasing Pressure Test (MIPT) loading conditions are considered. Two loading rates are considered: 0.1 MPa/s and 100 MPa/s. Only one Monte-Carlo run has been considered here for each calculation. To compare clearly the effect of the speed effect the same Monte-Carlo run has been used for these two calculations.

The second analysis carried out gives an answer to the previous questions concerning the scatter of the time to burst of the vessel. The different steps of the analysis are then as follows:

- Step 0 - Creation of 20 Monte-Carlo runs R_i $(i = 1, \ldots, 20)$;
- Step 1a - MIPT loading - Twenty calculations have been made, each using R_i, for the same MIPT loading. For each of these calculations, the failure (numerical instability) point of the vessel has been determined and then the burst pressures $P^{(i)}_{MIPT}$ corresponding to the i-th realisation of the Monte-Carlo process have been found;
- Step 1b - Find the median burst pressure in the case of MIPT loading - The 20 values of burst pressure $P^{(i)}_{MIPT}$ $(i = 1, \ldots, 20)$ allow the two parameters of the Weibull distribution of the burst pressures of the vessels under MIPT loading type (the maximum likelihood method has been used), denoted as W_{MIPT}, to be determined. In particular, the median burst pressure denoted $P^{(median)}_{MIPT}$ (defined with W_{MIPT} for a probability equal to 0.5) has been determined. Here, $P^{(median)}_{MIPT} = 272.45$ MPa;
- Step 2 - Six values of pressure, denoted as $P^{(J)}_{MISPT}$ $(J = 1, \ldots, 6)$, for Monotonic Increasing then Sustained Pressure Test (MISPT) have been chosen (to reach failure in a short period of

time, to save computational calculation time and also, if necessary, experimental test time). These values are: 245, 250, 255, 260, 265 and 270 MPa corresponding respectively to 89.9, 91.8, 93.6, 95.4, 97.3, and 99.1 % of $P_{MIPT}^{(median)}$;

- Step 3(J) MISPT loading at $P_{MISPT}^{(J)}$ $(J = 1, \ldots, 6)$ - 20 MISPT loading type calculations have been made with $P_{MISPT}^{(J)}$, each using R_i (R_i is the same as in the MIPT case). For each of these calculations, the failure (numerical instability) point of the vessel has been determined and then the time-to-failure $t_{MISPT}^{(J/i)}$ corresponding to R_i has been found. These 20 values of time-to-failure $t_{MISPT}^{(J/i)}$ allow determination of the two parameters of the Weibull distribution of the time-to-failure of the vessel under MISPT loading type (the maximum likelihood method has been used) with the pressure $P_{MISPT}^{(J)}$, denoted as $W_{MISPT}^{(J)}$.

11.3. Results of the calculations

The conclusions that can be made in the case of the pressure vessels are exactly the same as in the case of the unidirectional specimen, concerning, the effect of loading rate and clustering effect. In particular, as the speed of pressurisation increases so does the burst pressure. Figure 15 shows the calculated deformation of a pressure vessel as the pressure is increased and reveals very analogous behaviour as to that shown in the model described above with a failure initiation point $SINST$ reached just before the failure point. The burst pressure is shown to be lower with a reduced pressurisation rate, as has been shown to be the case experimentally [9]. Using the model it is shown that time to failure when the pressure vessel is pressurised, to different percentages of monotonic burst pressure, increases rapidly as the applied pressure is reduced, as shown in Figure 17. The scatter in lifetimes can be seen to increase as the mean lifetime increases with decreasing pressures. Using these results it can be seen that the curve is asymptotic to a threshold below which failure would not occur. This value is for a pressure level of approximately 80%. This is likely to be a conservative value given the assumptions made in the model and gives a value for an intrinsic safety value of 1.25 meaning that the intrinsic in-service pressure could be as high as 80% burst pressure. However, as emphasised above, this is based on the intrinsic properties of the composites and of its components (fibres and matrix). It does not take account of manufacturing defects or accidental loadings such as impacts.

We wish to determine:

- the scatter for the loading curve $< u_r >$ as a function of the applied pressure (or time because the applied pressure is a linear function of the time) in the case of the MIPT type loading (Fig. 16a);

- the scatter for the loading curve $< u_r >$ as a function of the time in the case of the MISPT type loading (Fig. 16b1-b6) for each of the sustained pressures $P_{MISPT}^{(J)}$ $(J = 1, \ldots, 6)$;
- if the scatter in the time-to-failure depends on the level of the sustained pressure (Fig. 17) in the case of MISPT loading;
- if the Monte-Carlo realisations which give the lowest and highest values of burst pressure in the MIPT loading case are the same as those which give the shortest and longest times-to-failure in the MISPT loading cases for each level of pressure (Fig. 18). If this is not the case, as already discussed in a previous paper, the same kinetics of fibre failure phenomena cannot be assumed to induce the failure of the vessel.

It shows :

- the scatter of $< u_r >_{liner}$ increases when the sustained pressure increases (Fig. 16);
- the scatter of the time-to-failure depends on the level of the sustained pressure: the scatter of the time-to-failure increases when the sustained pressure decreases (Fig. 17). This conclusion obtained with pressure vessels is the same as for simple unidirectionnal specimens [52] [58];
- for a given Monte-Carlo run R_i, it seems there is not a (direct) link between the time-to-failures obtained for each level of sustained pressure (Fig. 18).

For the last point, some details can be given. Each one of 20 Monte-Carlo values has been used seven times (one for monotonic loading and six for sustained constant loading. For each of the six steady loadings the time-to-failure of the twenty tests has been obtained and then ranked in increasing value (the first classed as being the shortest time-to-failure and the last corresponded to the longest survival time. In this way it is possible to determine if it is always the same Monte-Carlo distribution which gives the shortest time-to-failure for all steady pressures considered. Figure 18 shows the results and clearly this is not the case. It appears that the Monte-Carlo simulation gives random results from the twenty calculations made for each of the six steady loads considered. In other terms it is not always the same Monte-Caro simulation which gives the shortest or the longest time-to-failure for the maintained loads.

The time-to-failure depends on the level of steady pressure applied but also on the statistical variations due to the microstructure. This allows a curve of the maintained pressure level, which is a function of the statistical variations at the level of the fibres, to be drawn and to allow the value of the probability of failure to be quantified. In this study we have investigated the probability

curve for one failure in a million (Fig. 17c). In this way we can see that for a lifetime of four months the pressure should not exceed 86% of the monotonic burst pressure.

One of the important result of this study is that by using simulations of a relevant model, it is now possible to quantify the intrinsic safety factor of the composite material. In this study, the part of material safety factor found is that associated with the stochastic character of the fibre strength. This is considered likely to be the most important factor but it should be completed by the effect associated with the stochastic character of the fibre volume fraction.

The scatter in the local fibre volume fraction that can exist is also certainly important (as in case of simple specimens [52]). For now, though, this has not been taken into account.

However, it should be understood that to be able to define a safety factor for the structure other mechanisms must be considered such as defects induced by the manufacturing process, including porosity.

12. Conclusion

The object of this review has been to explore the mechanisms of failure in composite materials. Although the discussions are clearly relevant to all composites, it is the behaviour of carbon fibre reinforced matrices which has preoccupied most of the thinking described. There are several reasons for this: carbon fibres represent the fibre reinforcements with the highest performance; they are elastic and seemingly there are no mechanisms which cause their delayed failure, at least at room temperature. They are also the materials which are used for the most demanding of applications. The emphasis has been on the most widely used arrangements of fibre reinforcements in which they play the most important role in supporting the loads applied to a composite structure. In the simplest structure, that of a unidirectional composite with a typical fibre volume fraction of 60%, the fibres support approximately 99% of the load in the fibre direction. It has been shown experimentally, however, that the properties of such a composite under load, unlike the individual fibres, are time dependent due to the viscoelastic behaviour of the matrix. This clearly has implications for their long term use. As the fibres support the greatest part of the load their failure represents the most damaging damage process which can occur in a composite structure. A multiscale model has been presented which is based on physical processes including fibre failure and load transfer through the matrix to induce increased loads in intact fibres neighbouring fibre breaks which can lead to progressive fibre failure. The multi-scale model presented considers failure at the level of the constituents, the fibres, the matrix and their interfaces and it is shown how using

this information can simulate the behaviour of the macroscopic composite structure. Given the numbers of fibres making up a composite structure it is necessary to reduce computing times to reasonable levels. To do this the most damaging cases are considered so as to obtain a conservative evaluation of its macroscopic behaviour. This is shown to reflect accurately the tensile behaviour of both unidirectional composites loaded in the fibre direction and also filament wound pressure vessels under load. The viscoelastic nature of the matrix introduces time into the behaviour of the composite structures and this is accurately shown to correspond closely to experimental results obtained on both types of composite structure. The model has been applied to filament wound structures with the objective of examining the time dependent behaviour of pressure vessels. It has been shown that the burst pressure of a carbon fibre pressure vessel decreases as pressurisation rate is lowered which agrees with experimentally observations. Failure under steady loads has been studied both experimentally and theoretically in order to examine the effects of using pressure vessels over long periods of time. This approach has enabled safety factors to be quantified for these structures based on the real intrinsic damage processes which occur in composites. In the case of carbon fibre composite pressure vessels the minimum safety factor has been determined to be around 1.25, although it should be emphasised that this is based on the intrinsic properties of the material and does not take into account manufacturing errors and damage such as by impact.

13. And after...

Multi-scale models are mainly based on the studies of Suquet [59] and Lene [60]. From the beginning of the present century these techniques have acquired general acceptance for their wide use and implementation in calculation codes [12] as they show an excellent correspondence to theoretical concepts. They do have, however, the disadvantage of requiring long calculation times. Improvements which have been made have concentrated on reducing the costs involved in the calculations and have for that reason tend to use non-general assumptions. It has seemed to the present authors that rather than continuing the development of models which are of necessity less robust than the original, the general approach should be employed to obtain conclusions which cannot be, for now, directly accessible by experiment, as has been made in this study. However in that case the calculations would be extremely long and would have to be repeated so as to examine the effects of stochastic behaviour. This has meant that another approach has been adopted to reduce the calculation times. This may seem to contradict what we have just written above. In reality it is not. The length of our calculations is due to two things: the first one is that one single calculation is very long, the second one is that we have to do it several times to examine the stochastic character of the results. So, we sought to reduce the size of the area within the structure

necessary to obtain of a reliable calculation: initially, the whole structure was considered and now, by invoking the concepts of statistical ergodic random functions [61] [62] [63] [64] this area has been reduced. As a consequence, the same quality of results is preserved but the computation time is drastically reduced. We have thus not degraded the multiscale process but only the size of the area where it operates [65].

[1] J. Johnson, W. Watt, L. Phillips, R. Moreton, Improvements in or relating to carbonisable fibre and carbon fibre and their production, U.K. Patent 1-166-251.

[2] J. Johnson, W. Watt, L. Phillips, R. Moreton, Carbon fibre reinforced plastics. the first fifteen years, Plastics and rubber Int. 3 (6) (1978) 239–246.

[3] A. Bunsell, A. Somer, The tensile and fatigue behaviour of carbon fibres, Plastics, rubber and composites processing and applications 18 (1992) 263–267.

[4] M. Fuwa, A. Bunsell, B. Harris, An evaluation of AE techniques applied to carbon fibre composites, Journal of physics D : applied physics 9 (1976) 353–364.

[5] D. Laroche, Accumulation d'endommagement dans le carbone époxyde détecté par émission acoustique, Thèse, Ecole des Mines de Paris, 1980.

[6] D. Laroche, A. Bunsell, Stress and time dependent damage in carbon fibre reinforced plastics, In: Advances in Composite Materials, Bunsell A.R. Ed. vol. 2 (1980) 985–997.

[7] A. Bunsell, D. Laroche, V. D., Damage and failure in carbon-fiber-reinforced epoxy resin, In: Long-term behavior of composites, O'Brien T.K. Ed. ASTM STP 813 (1983) 38–54.

[8] J. Lifschitz, A. Rotem, Time-dependent longitudinal strength of unidirectional fibrous composites, Fibre science and technology 3 (1970) 1–20.

[9] H. Chou, A. Bunsell, G. Mair, A. Thionnet, Effect of the loading rate on ultimate strength of composites. Application: Pressure vessel slow burst test, Composites Structures 104 (2013) 144–153.

[10] F. Islam, S. Joannès, S. Bucknell, Y. Leray, A. Bunsell, L. Laiarinandrasana, Investigation of tensile strength and dimensional variation of t700 carbon fibres using an improved experimental setup, Reinforced plastics and Composites 39 (2020) 144–162.

[11] K. Gan, M. Wisnom, S. Hallet, Effect of high through-thickness compressive stress on fibre direction tensile strength of carbon/epoxy composite laminates, Composites Science and Technology 90 (2014) 1–18.

[12] F. Feyel, A multilevel finite element method (FE2) to describe the response of highly non-linear structures using generalized continua, Computer Methods in applied Mechanics and engineering 192 (2003) 3233–3244.

[13] A. Thionnet, J. Renard, Multi-scale analysis to determine fibre/matrix debonding criteria in SiC/Titanium composites with and without consideration of the manufacturing residual stresses, Composites Science and Technology 58 (1998) 945–955.

[14] F. Souza, D. Allen, Y. Kim, Multiscale model for predicting damage evolution in composites due to impact loading, Composites Sciences and Technology 68 (2008) 2624–2634.

[15] S. Blassiau, Modélisation Des Phénomènes Microstructuraux Au Sein d'un Composite Unidirectionnel Carbone/Époxy et Prédiction de Durée de Vie : Contrôle et Qualification de Réservoirs Bobinés, Thèse, Ecole des Mines de Paris, 2005.

[16] S. Blassiau, A. Thionnet, A. Bunsell, Micromechanisms of load transfert in a unidirectional carbon-fibre epoxy composite due to fibre failures. Part 1: Micromechanisms and 3D analysis of load transfert, the elastic case, Composite Structures 74 (2006) 303–318.

[17] S. Blassiau, A. Thionnet, A. Bunsell, Micromechanisms of load transfert in a unidirectional carbon-fibre epoxy composite due to fibre failures. Part 2: Influence of viscoelastic and plastic matrices on the mechanism of load transfert, Composite Structures 74 (2006) 319–331.

[18] S. Blassiau, A. Thionnet, A. Bunsell, Micromechanisms of load transfert in a unidirectional carbon-fibre epoxy composite due to fibre failures. Part 3: Multiscale reconstruction of composite behaviour, Composite Structures 83 (2008) 312–323.

[19] B. Rosen, Tensile failure of fibrous composites, AIAA journal 2 (1964) 1985–1991.

[20] H. Cox, The elasticity and strength of paper and other fibrous materials, British journal of applied physics 12 (1951) 72–79.

[21] C. Zweben, Tensile failure of fibers composites, AIAA journal 6 (1968) 2325–2331.

[22] J. Hedgepeth, Stress Concentrations in Filamentary Structures, Rapport, NASA TND882, Langley research center, 1961.

[23] S. Ochiai, K. Schulte, P. Peters, Strain concentration for fibers and matrix in unidirectional composites, Composites science and technology 41 (1991) 237–256.

[24] W. Curtin, Dimensionality and size effects on the strength of fiber-reinforced composites, Composites Sciences and Technology 60 (2000) 543–551.

[25] W. Curtin, N. Takeda, Tensile strength of fiber-reinforced composites: I. model and effects of local fiber geometry, Journal of composite materials 32 (1998) 2042–2059.

[26] W. Curtin, M. Ibnabdeljalil, Strength and reliability of fiber-reinforced composites: Localized load sharing and associated size effects, International Journal of Solids and structures 34 (1997) 2649–2668.

[27] J. Goree, R. Gross, Stresses in a three-dimensional unidirectional composite containing broken fibers, Engineering fracture mechanics 13 (1980) 395–405.

[28] D. Harlow, S. Phoenix, The chain-of-bundles probability model for the strength of fibrous materials 1: Analysis and conjectures, Journal of composite materials 12 (1978) 195–213.

[29] D. Harlow, S. Phoenix, The chain-of-bundles probability model for the strength of fibrous materials 2: A numerical study of convergence, Journal of composite materials 12 (1978) 314–334.

[30] P. Scop, A. Argon, Statistical theory of strength of laminated composites, Journal of composite materials 1 (1967) 92–99.

[31] P. Scop, A. Argon, Statistical theory of strength of laminated composites 2, Journal of composite materials 3 (1969) 30–44.

[32] P. Kong, A Monte carlo study of the strength of unidirectional fiber-reinforced composites, Journal of composite materials 13 (1979) 311–327.

[33] S. Batdorf, Tensile strength of unidirectionally reinforced composites - 1, Journal of reinforced plastics and composites 1 (1982) 153–163.

[34] S. Batdorf, Tensile strength of unidirectionally reinforced composites - 2, Journal of reinforced plastics and composites 1 (1982) 165–175.

[35] M. Nedele, M. Wisnom, Three dimensional finite analysis of the stress concentration at a single fibre break, Composites science and technology 51 (1994) 517–524.

[36] M. Nedele, M. Wisnom, Stress concentration factors around a broken fibre in a unidirectional carbon fibre-reinforced epoxy, Composites 25 (1994) 549–557.

[37] J. Hedgepeth, P. V. Dyke, Local stress concentrations in imperfect filamentary composite materials, Journal of composite materials 1 (1967) 294–309.

[38] C. Baxevanakis, Comportement Statistique à Rupture Des Composites Stratifiés, Thèse, Ecole des Mines de Paris, 1994.

[39] C. Landis, R. McMeeking, Stress concentrations in composites with interface sliding, matrix stiffness and uneven fiber spacing using shear lag theory, International journal of solids and structures 36 (1999) 4333–4361.

[40] C. Landis, I. Beyerlein, R. McMeeking, Micromechanical simulation of the failure of fiber reinforced composites, Journal of the mechanics and physics of solids 48 (2000) 621–648.

[41] S. Phoenix, Statistical issues in the fracture of brittle matrix fibrous composites: Localized load-sharing and associated size effects, International Journal of Solids and Structures 34 (1997) 2649–2668.

[42] S. Phoenix, I. Beyerlein, Statistical strength theory for fibrous composite materials, in Comprehensive composite materials Pergamon-Elsevier Science, A. Kelly and C. Zweben editors (2000) 559–639.

[43] S. Phoenix, W. Newman, Time-dependent fiber bundles with local load sharing. II. General Weibull fibers, Physical Review 80 (2009) 066115.

[44] S. Mahesh, S. Phoenix, Lifetime distributions for unidirectional fibrous composites under creep-rupture loading, International journal of fracture 127 (2004) 303–360.

[45] M. Wisnom, D. Green, Tensile failure due to interaction between fibre breaks, Composites 26 (1995) 499–508.

[46] P. Van Den Heuvel, S. Goutianos, R. Young, T. Peijs, Failure phenomena in fibre-reinforced composites Part 6: A finite element study of stress concentrations in unidirectional cfr epoxy composites, Composites science and technology 64 (2004) 645–656.

[47] P. Van Den Heuvel, M. Wubbolts, R. Young, T. Peijs, Failure phenomena in two-dimensional multi-fibre model composites: 5. A finite element study, Composites A 29 (1998) 1121–1135.

[48] D. Lagoudas, C. Hui, S. Phoenix, Time evolution of overstress profiles near broken fibers in a composite with a viscoelastic matrix, International journal of solids and structures 25 (1989) 45–66.

[49] I. Beyerlein, C. Zhou, L. Schadler, Time evolution of stress redistribution around multiple fiber breaks in a composite with viscous and viscoelastic matrices, International journal of solids and structures 35 (1998) 3177–3211.

[50] S. Camara, A. Bunsell, A., D. Allen, Determination of lifetime probabilities of carbon fibre composite plates and pressure vessels for hydrogen storage, International Journal of Hydrogen Energy 36 (2011) 6031–6038.

[51] A. Scott, I. Sinclair, S. Spearing, A. Thionnet, A. Bunsell, Damage accumulation in a carbon/epoxy composite: Comparison between a multiscale model and computed tomography experimental results, Composites Part A 43 (2012) 1514–1522.

[52] H. Chou, A. Thionnet, A. Mouritz, A. Bunsell, Stochastic factors controlling the failure of carbon/epoxy composites, Journal of Materials Science 51 (1) (2015) 311–333. doi:10.1007/s10853-015-9390-5.

[53] A. Bunsell, D. Valentin, Towards a life prediction technique for carbon fibre filament wound structures subjected to steady pressures, Composite structures 1 (1983) 67–81.

[54] J. Rojek, Improvement of a fibre break model in a vue of an improvement of the security design of composite pressure vessels, Thèse, PSL - Mines Paristech, France, 2020.

[55] Y. Swolfs, I. Verpoest, L. Gorbatikh, Issues in strength models for unidirectional fibre-reinforced composites related to weibull distributions, fibre packings and boundary effects, Composites Science and Technology 114 (2015) 42–49.

[56] J. Aveston, G. Cooper, A. Kelly, Single and multiple fracture, the properties of fibre composites, Proc. Conf. National Physical Laboratories IPC Sci. and Tech Press Ltd., London (1971) 15–24.

[57] J. Aveston, A. Kelly, Theory of multiple fracture of fibrous composites, Journal of Material Sciences 8 (1973) 352–362.

[58] A. Bunsell, A. Thionnet, H. Chou, Intrinsic safety factors for glass and carbon fibre composite filament wound structures, Applied Composite Materials 21 (1) (2014) 107–121. doi:10.1007/s10443-013-9367-y.

[59] P. Suquet, Plasticité et homogénéisation, Thèse d'état, Université Paris VI, 1982.

[60] F. Léné, Contribution à l'étude des matériaux composites et de leur endommagement, Thèse d'état, Université Paris VI, 1984.

[61] G. Matheron, Elements pour une theorie des milieux poreux, Masson, Paris, 1967.

[62] G. Matheron, Random Sets and Integral Geometry, Wiley, New-York, 1975.

[63] C. Lantuejoul, Ergodicity and integral range, Journal of Microscopy 161 (1991) 387–403.

[64] V. Svetlitsky, Stationary Random Functions (Processes). In: Statistical Dynamics and Reliability Theory for Mechanical Structures. Foundations of Engineering Mechanics, Springer, 2003.

[65] M. Widjaja, S. Joannès, A. Bunsell, G. Mair, A. Thionnet, The application of a reduced volume method for the simulation of the characterisation of a carbon fibre pressure vessel, ECCM 2018 - 18th European Conference on Composite Materials, 2020.

[66] H. Chou, Accumulation d'endommagement dans les unidirectionnels carbone/époxy sous chargements maintenus, Rapport interne, Ecole des Mines de Paris, 2016.

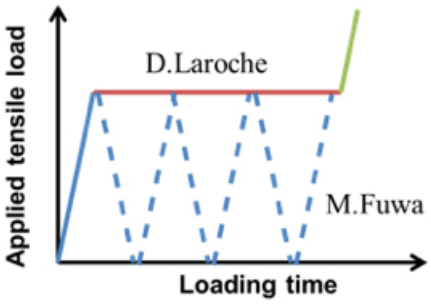

Figure 1: Constant load cycling and also steady loading of unidirectional carbon fibre composites showed that damage accumulated which could lead to their failure.

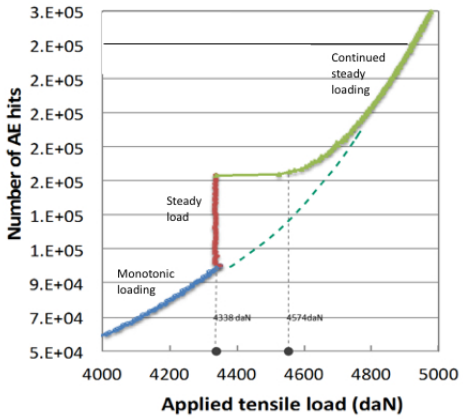

Figure 2: Monotonic loading of a unidirectional carbon fibre composite loaded in the fibre direction leads to damage accumulation. This zoom of part of the loading curve shows that damage continues to increase when the loading is stopped and held steady. Resuming the monotonic loading initially results in much reduced rate of damage until the extrapolated initial curve is reached.

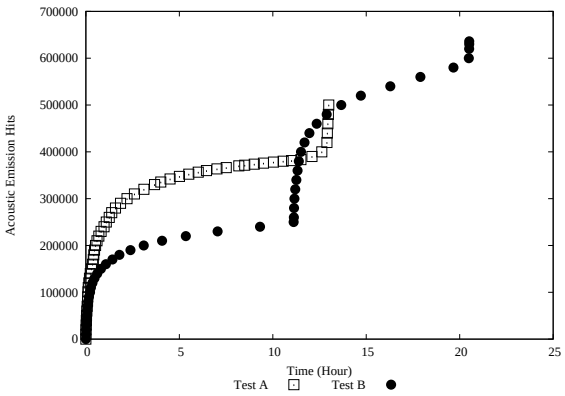

Figure 3: A unidirectional carbon fibre composite loaded in the fibre direction to 96% of its nominal failure load and sustained [66]. Two tests have been carried out until failure of the specimens, under the same experimental conditions. The last point of each curve correspond to the end of the recording of Acoustic Emission Events because of the failure of the specimen. For Test A, after a progressive evolution of damage, the damage accecelerates suddenly until failure ($\approx$ 12 hours). For Test B, after a progressive evolution of damage, a first point ($\approx$ 11 hours) shows that the damage accecelerates suddenly but stopped its accelaration ($\approx$ 12 hours), to re-accelerates at a second point ($\approx$ 21 hours) until failure.

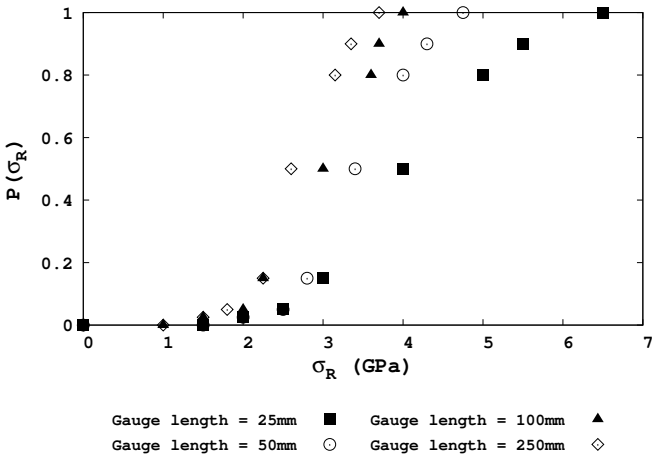

Figure 4: Typical experimental cumulative probability $P(\sigma_R)$ for carbon fibre strength σ_R [15].

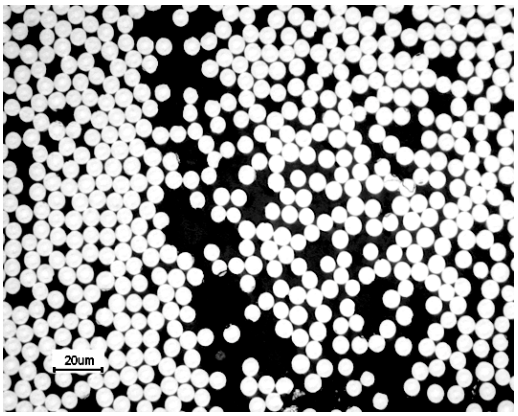

(a)

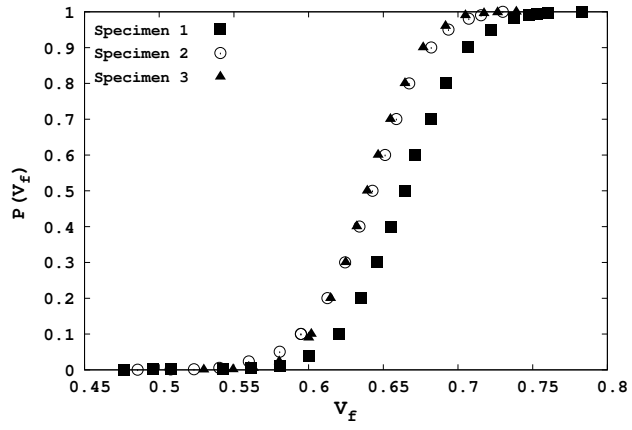

(b)

Figure 5: (a) Typical micrography of (0°) carbon/epoxy specimen. (b) Typical experimental cumulative probability of fibre volume fraction for three (0°) carbon/epoxy specimens coming from the same plate.

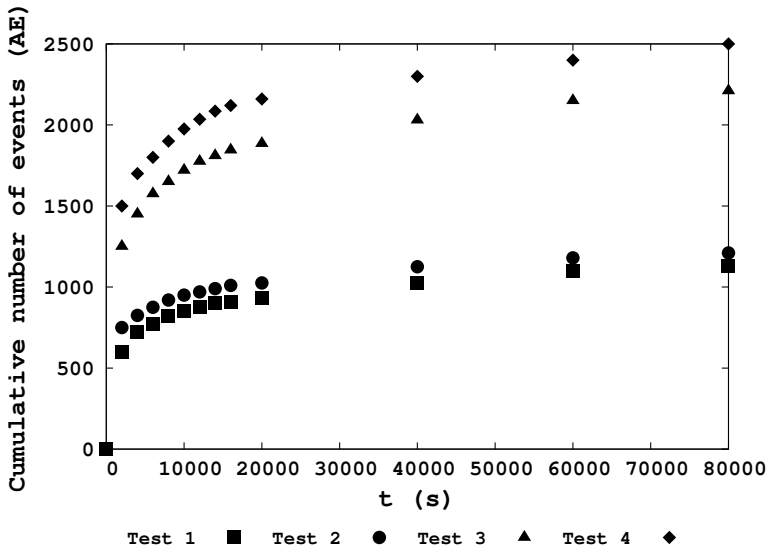

(a)

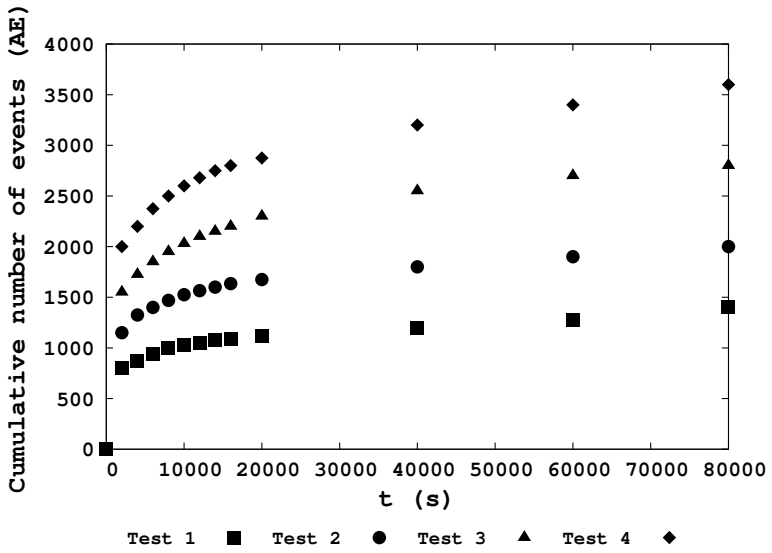

(b)

Figure 6: Experimental scatter of cumulative number of events obtained by Acoustic Emission for (0°) carbon/epoxy specimens under sustained loading at X % of the failure strength of the specimen [15]. (a) $X = 75\%$. (b) $X = 80\%$. One Acoustic Emission Event (AE) is assumed to be one fibre break.

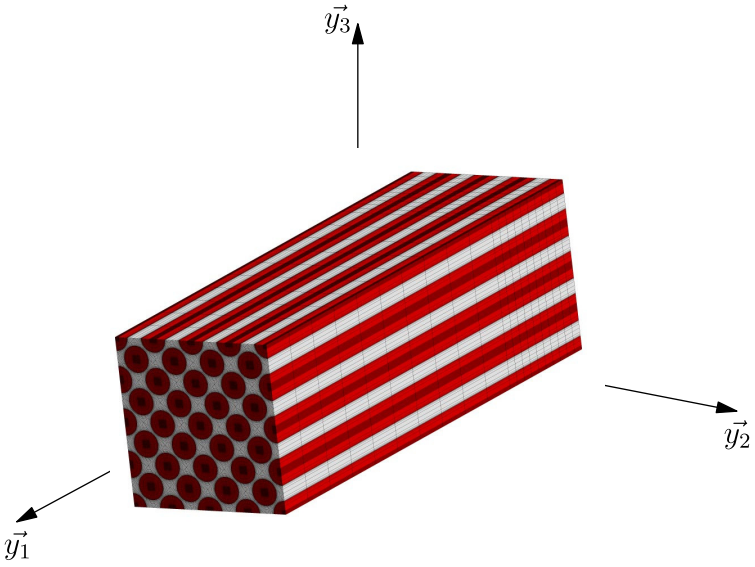

Figure 7: Representative Volume Element (RVE) of a unidirectional composite showing the fibres embedded in the resin matrix. Associated framework at the microscopic scale: $R_y = (O_y, \vec{y_1}, \vec{y_2}, \vec{y_3})$.

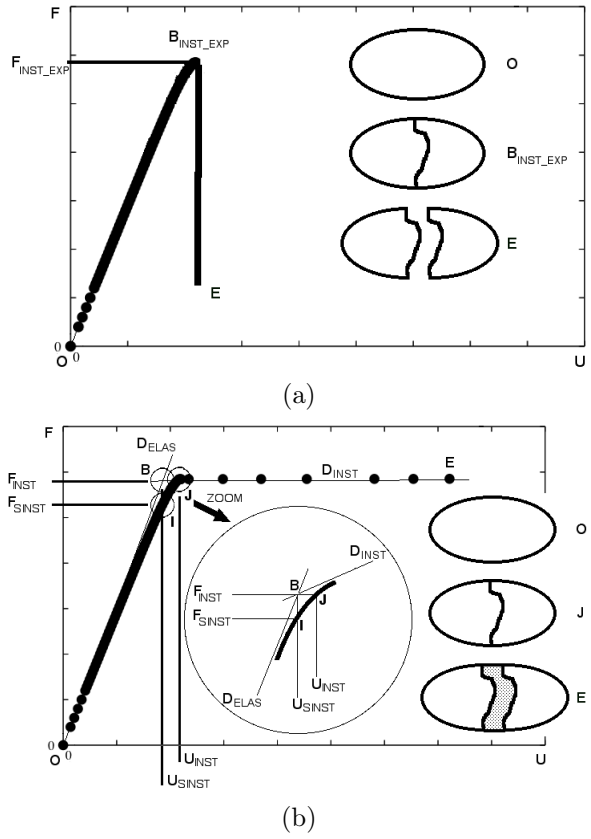

Figure 8: Definition of the failure point of a structure. (a) Typical experimental loading curve of a structure until failure highlighting the experimental instability point B_{INST_EXP} defining the break into two parts of the structure. This is also a typical simulated curve of a structure until failure, made in the Fracture Mechanics framework. In both cases, the failure of the structure is induced by the breakage into two parts of the structure showing discontinuities of displacement in a created surface. (b) Typical simulated loading curve of a structure in the framework of the Damage Mechanics highlighting the numerical instability starting at the Start of INStability Point I and assumed to finish at J (Failure Point or Instability Point) close to the real breakage into two parts of the structure.

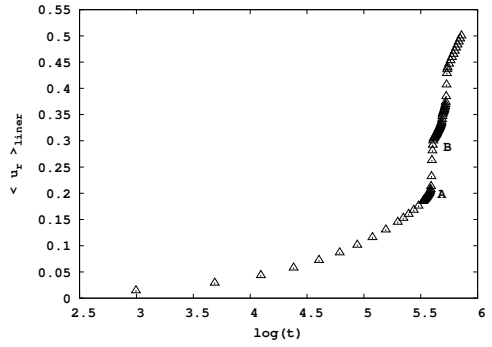

(a)

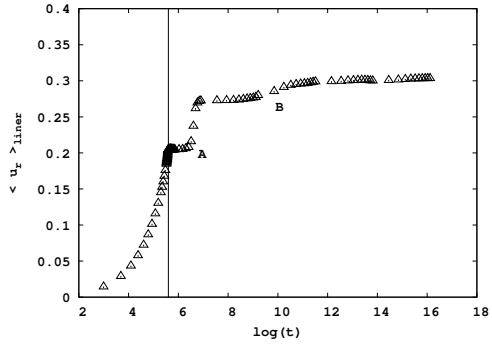

(b)

Figure 9: Typical loading curves for Monotonic Increasing Pressure Test (MIPT) and Monotonic Increasing then Sustained Pressure Test (MISPT) for a pressure vessel: averaged, over the liner, of the radial displacement u_r as a function of the time, i.e., $< u_r >_{liner}$ versus t or $log(t)$. (a) Monotonic Increasing Pressure Test until failure. The Point A defines the first instability point of the loading curve. The Point B is another instability point. From a security point of view, the Point A is taken as the failure point of the vessel. (b) Monotonic Increasing then Sustained Pressure Tests until failure. After the monotonic part of the pressure loading (time before the vertical bar), the pressure P_{MISPT} was sustained for 4 months (10^7 seconds). The Point A defines the first instability point of the loading curve but it appear that the vessel was far from being separated into two parts. The Point B is another instability point, which does not always correspond to the total destruction of the vessel. From a security point of view, the Point A is taken as the failure point of the vessel. This type of curve can be explained similarly by the experimental measurement made on a simple specimen (Fig. 3): firstly, somewhere in the structure, suddenly, the damage grew but stopped (Point A); then, the time continues and again, somewhere in the structure, suddenly, the damage grew but stopped (Point B) but did not lead immediately to failure.

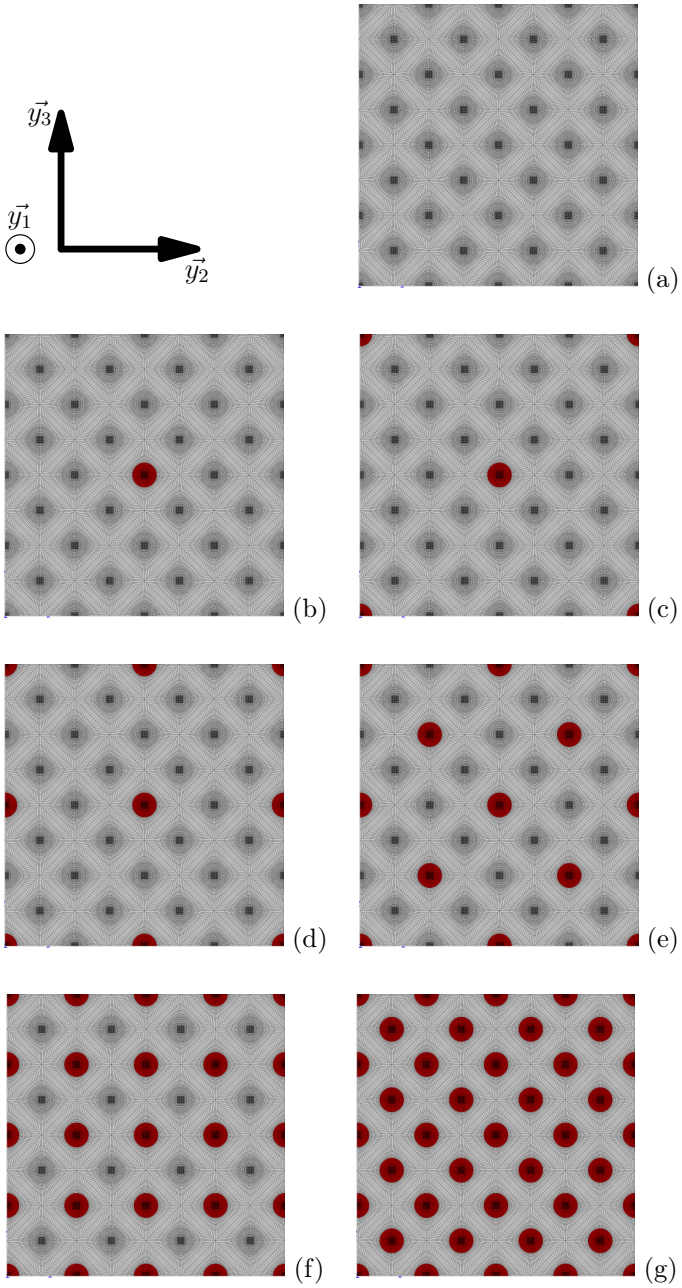

Figure 10: Representative Volume Element of the material damage states and corresponding i-plets. Broken fibres are in red colour. (a) RVE $CS32$ / 0-plet. (b) RVE $C32$ / 1-plet. (c) RVE $C16$ / 2-plet. (d) RVE $C8$ / 4-plet. (e) RVE $C4$ / 8-plet. (f) RVE $C2$ / 16-plet. (g) RVE $C1$ / 32-plet.

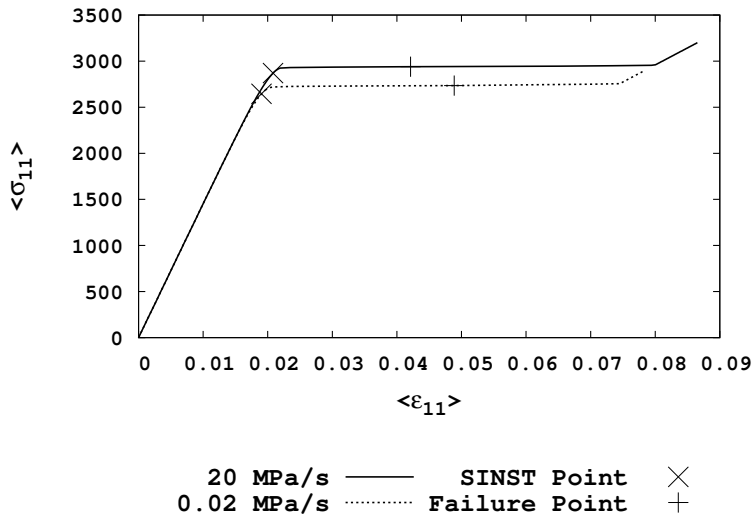

(a)

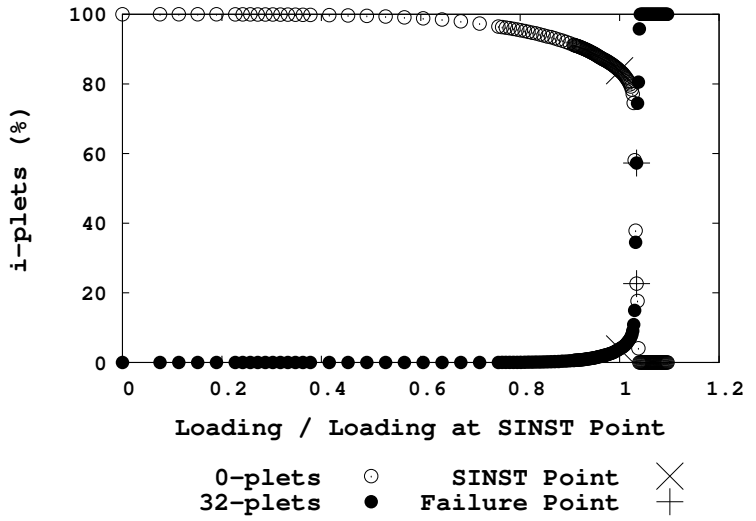

(b)

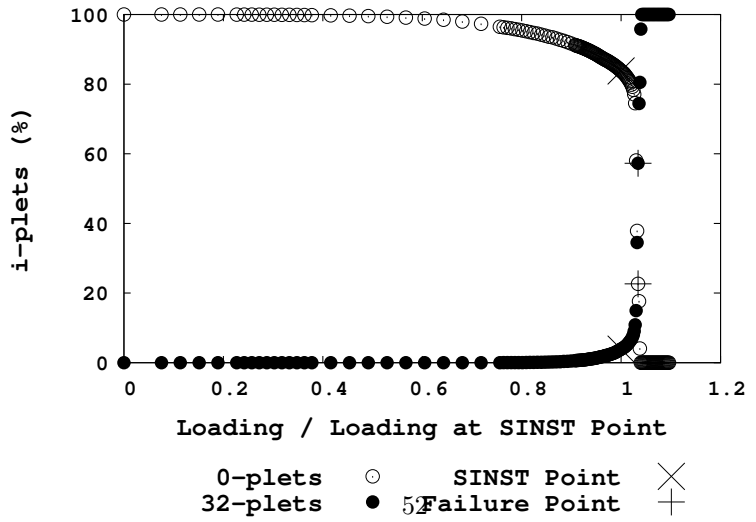

(c)

Figure 11: Simple specimen under monotonic loading increasing to failure (ML case). (a) Comparison of loading curves showing the influence of speed of loading. (b) Evolution of the populations of 0-plets and 32-plets (0.02 MPa/s). (c) Evolution of the populations of 0-plets and 32-plets (20.00 MPa/s).

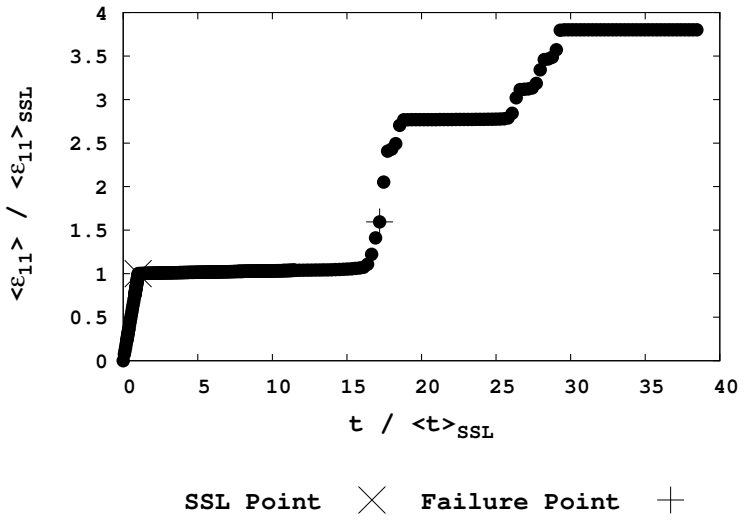

(a)

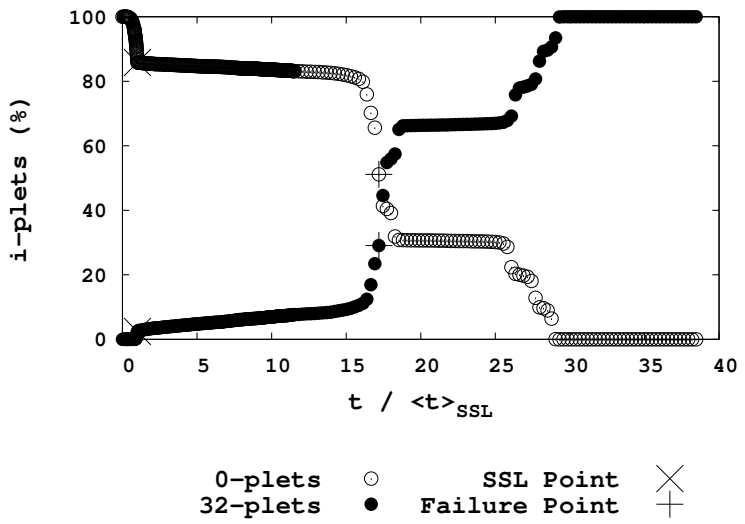

(b)

Figure 12: Simple specimen under increasing monotonic loading until held at a constant load until its eventual failure (SL case). (a) Loading curve showing $< e_{11} > / < e_{11} >_{SSL}$ strain in the fibre direction divided by strain at beginning of sustained loading. (b) Evolution of the populations of 0-plets and 32-plets representing clusters of fibre breaks.

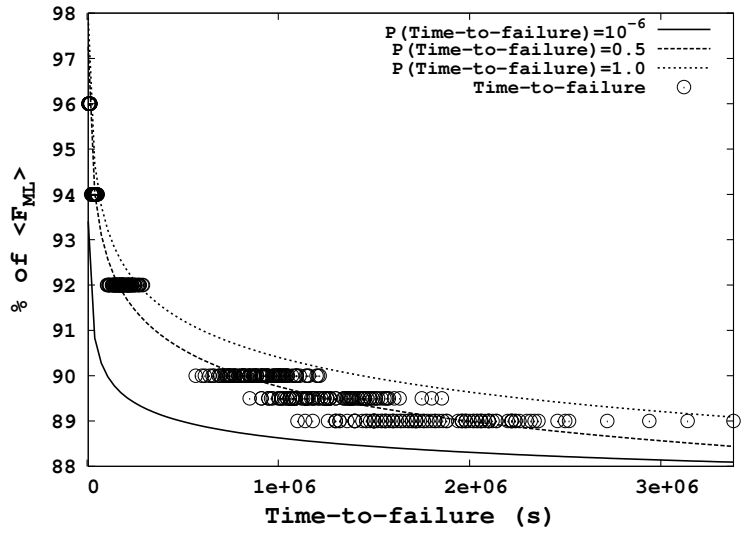

Figure 13: Simple specimen under increasing monotonic loading until held at a constant load until its eventual failure (SL case). Scatter of the time-to-failure for different sustained load levels ($X \times F^{MCR001}_{SINST\_20}$, X = 0.96, 0.94, 0.92, 0.90, 0.895, 0.89, 50 Monte-Carlo runs have been considered for each level).

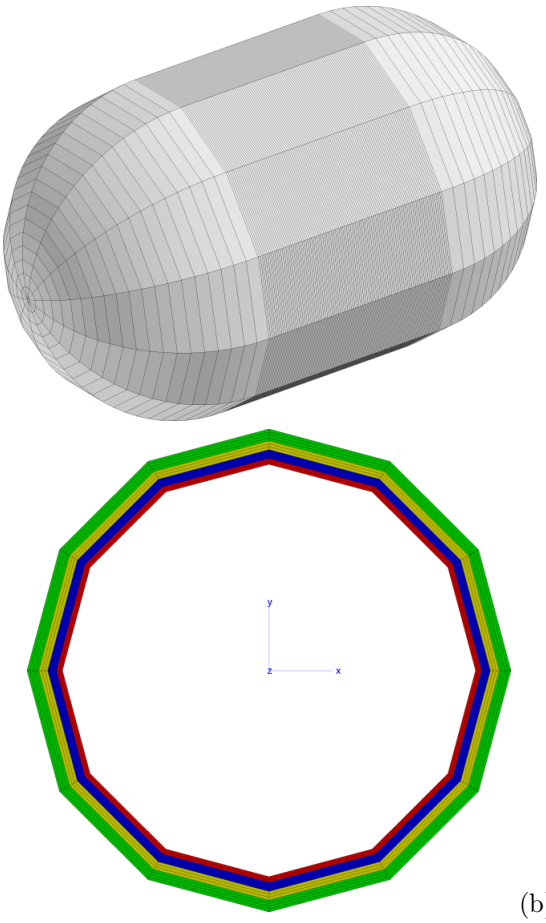

Figure 14: Simple pressure vessel considered for reasons of calculation time. (a) Mesh of the pressure vessel. (b) Mesh of the cross section of the pressure vessel (green: ply 1, 90° / yellow: ply 2, +20° / blue: ply 3, −20° / red: liner).

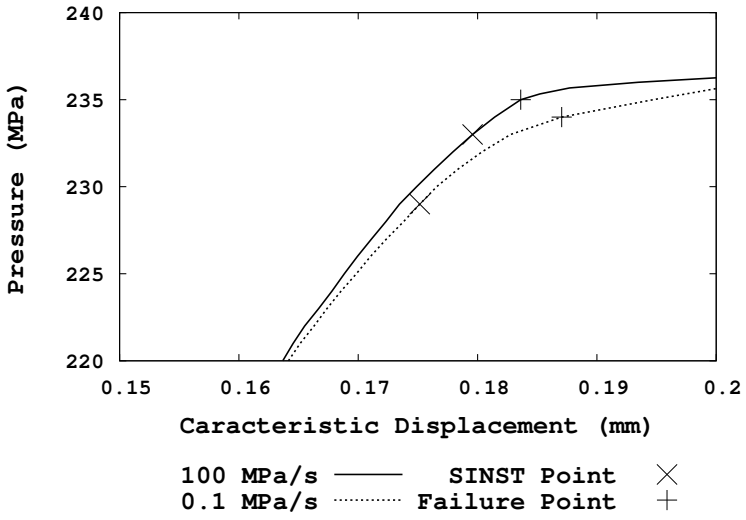

Figure 15: Simulation of a simplified pressure vessel subjected to increasing monotonic loading up to burst. Comparison of loading curves showing the influence of the speed of loading, as described in full size pressure vessels by Chou *et al.* [9].

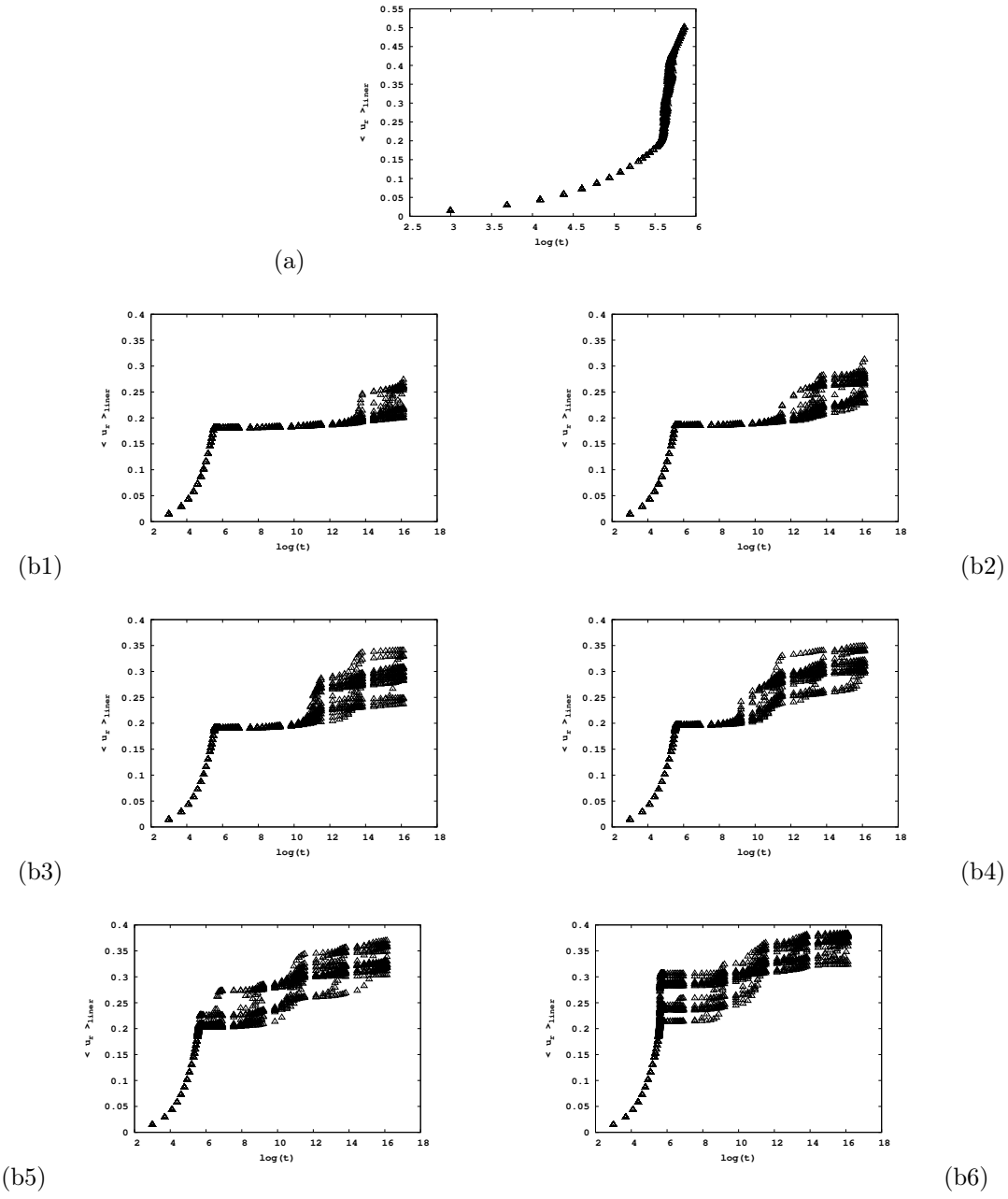

Figure 16: Loading curves of MIPT and MISPT cases: average, over the liner, of the radial displacement u_r as a function of the time t, i.e., $< u_r >_{liner}$ (mm) versus $log(t)$. (a) MIPT case. Monotonic increasing pressurization (1 MPa/s) until burst of the vessel. 20 loading curves coming each from one of the 20 different Monte-Carlo runs R_i are plotted. Each of these curves gives a burst pressure $P^{(i)}_{MIPT}$. The burst pressure $P^{(median)}_{MIPT}$ (= 272.45 MPa) is the median value for the burst pressure calculated using a maximum likelihood method for the 20 values $P^{(i)}_{MIPT}$. This value has been taken as the reference for the tests with sustained pressure levels. (b) MISPT case. Monotonic increasing pressurization (1 MPa/s) until $P_{SL} = P^{(J)}_{MISPT}$ equal to $X\%$ of $P^{(median)}_{MIPT}$ which was then simulated as being held constant for four months ($\approx 10^7$ seconds). For each value of the sustained pressure, 20 loading curves coming each from one of the 20 different Monte-Carlo runs R_i (the same as in the MIPT case) are plotted. Each of these curves gives a time-to-failure $t^{(J/i)}_{MISPT}$. (b1) $X = 89.9\%$, $P_{SL} = P^{(1)}_{MISPT} = 245$ MPa. (b2) $X = 91.8\%$, $P_{SL} = P^{(2)}_{MISPT} = 250$ MPa. (b3) $X = 93.6\%$, $P_{SL} = P^{(3)}_{MISPT} = 255$ MPa. (b4) $X = 95.4\%$, $P_{SL} = P^{(4)}_{MISPT} = 260$ MPa. (b5) $X = 97.3\%$, $P_{SL} = P^{(5)}_{MISPT} = 265$ MPa. (b6) $X = 99.1\%$, $P_{SL} = P^{(6)}_{MISPT} = 270$ MPa.

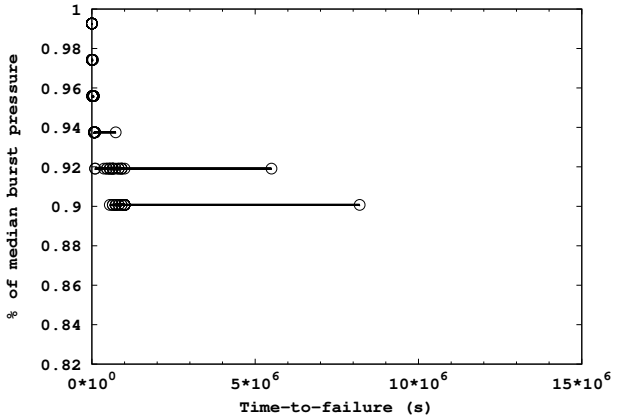

(a)

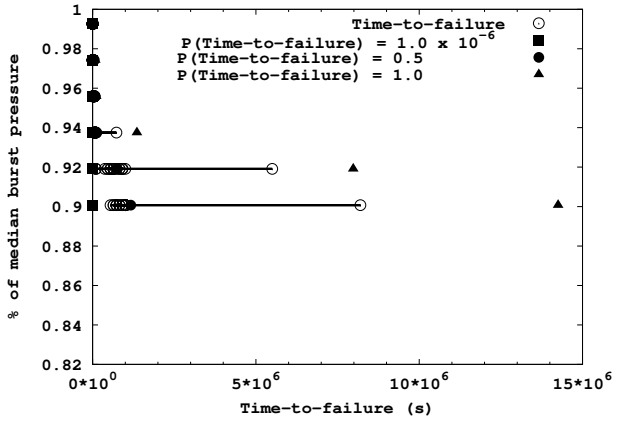

(b)

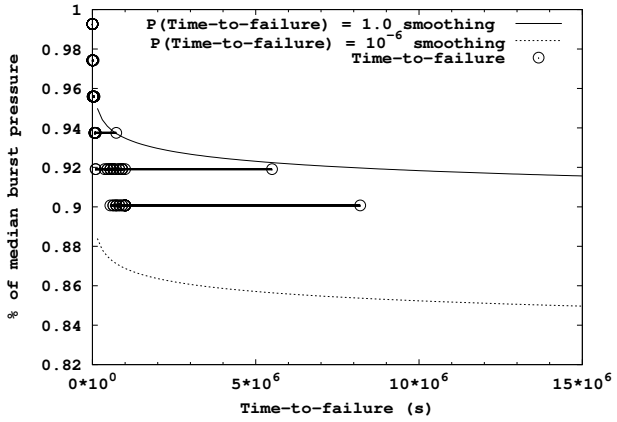

(c)

Figure 17: Analysis of the time-to-failure for each value of steady pressure. (a) For each value of steady pressure $P_{SL} = P^{(J)}_{MISPT}$ $(J = 1, ..., 6)$, the twenty values of time-to-failure $t^{(J/i)}_{MISPT}$ were obtained for each Monte-Carlo run R_i $(i = 1, ..., 20)$. The circles indicates the numerical results and the dark lines indicates the scatter obtained with these results. (b) For each value of maintained pressure $P_{SL} = P^{(J)}_{MISPT}$ $(J = 1, ..., 6)$, the twenty values of time-to-failure $t^{(J/i)}_{MISPT}$ allow the parameters of the Weibull distribution $W^{(J)}_{MISPT}$ to be calculated (using the maximum likelihood calculation) for the time-to-failure at this value of steady pressure. In this way, for each value of steady pressure it becomes possible to give the time-to-failure for a choosen probability. The probabilities of failure corresponding to one in a million to one hundred percent certainty have been plotted. (c) For each value of steady pressure $P_{SL} = P^{(J)}_{MISPT}$ $(J = 1, ..., 6)$, the twenty values of time-to-failure obtained have been plotted as well as the smoothed curves of time-to-failure for probabilities from one in a million to one hundred percent.

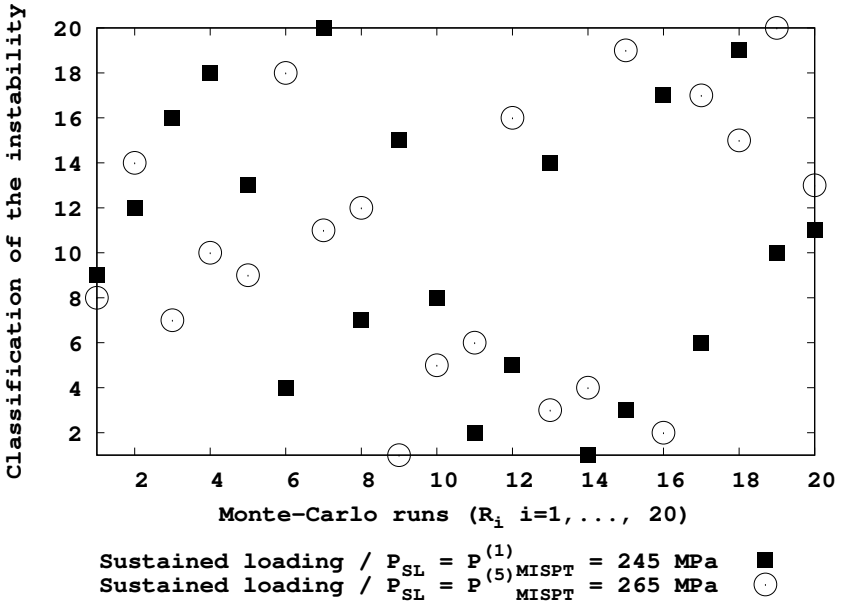

Figure 18: Ranking in increasing order of the twenty values of time-to-failure obtained for each Monte-Carlo runs for $P_{SL} = P^{(1)}_{MISPT} = 245$ Mpa and $P_{SL} = P^{(5)}_{MISPT} = 265$ Mpa. So that, for example, the R_9 Monte-Carlo run gives the shortest time-to-failure with a pressure of $P^{(5)}_{MISPT} = 265$ Mpa but gives the fifteenth time-to-failure for a pressure of $P^{(1)}_{MISPT} = 245$ Mpa.

Figure 1

Constant load cycling and also steady loading of unidirectional carbon fibre composites showed that damage accumulated which could lead to their failure.

Figure 2

Monotonic loading of a unidirectional carbon fibre composite loaded in the fibre direction leads to damage accumulation. This zoom of part of the loading curve shows that damage continues to increase when the loading is stopped and held steady. Resuming the monotonic loading initially results in much reduced rate of damage until the extrapolated initial curve is reached.

Figure 3

A unidirectional carbon fibre composite loaded in the fibre direction to 96% of its nominal failure load and sustained [66]. Two tests have been carried out until failure of the specimens, under the same experimental conditions. The last point of each curve correspond to the end of the recording of Acoustic Emission Events because of the failure of the specimen. For Test A, after a progressive evolution of damage, the damage accecelerates suddenly until failure ($\approx$ 12 hours). For Test B, after a progressive evolution of damage, a first point ($\approx$ 11 hours) shows that the damage accecelerates suddenly but stopped its accelaration ($\approx$ 12 hours), to re-accelerates at a second point ($\approx$ 21 hours) until failure.

Figure 4

Typical experimental cumulative probability $P(\sigma_R)$ for carbon fibre strength σ_R [15].

Figure 5

(a) Typical micrography of (0°) carbon/epoxy specimen. (b) Typical experimental cumulative probability of fibre volume fraction for three (0°) carbon/epoxy specimens coming from the same plate.

Figure 6

Experimental scatter of cumulative number of events obtained by Acoustic Emission for (0°) carbon/epoxy specimens under sustained loading at X % of the failure strength of the specimen [15]. (a) $X = 75\%$. (b) $X = 80\%$. One Acoustic Emission Event (AE) is assumed to be one fibre break.

Figure 7

Representative Volume Element (RVE) of a unidirectional composite showing the fibres embedded in the resin matrix. Associated framework at the microscopic scale: $R_y = (O_y, \vec{y_1}, \vec{y_2}, \vec{y_3})$.

Figure 8

(a) Typical experimental loading curve of a structure until failure highlighting the experimental instability point B_{INST_EXP} defining the break into two parts of the structure. This is also a typical simulated curve of a structure until failure, made in the Fracture Mechanics framework. In both cases, the failure of the structure is induced by the breakage into two parts of the structure showing discontinuities of displacement in a created surface. (b) Typical simulated loading curve of a structure in the framework of the Damage Mechanics highlighting the numerical instability starting at the Start of INStability Point I and assumed to finish at J (Failure Point or Instability Point) close to the real breakage into two parts of the structure.

Figure 9

Typical loading curves for Monotonic Increasing Pressure Test (MIPT) and Monotonic Increasing then Sustained Pressure Test (MISPT) for a pressure vessel: averaged, over the liner, of the radial displacement u_r as a function of the time, i.e., $< u_r >_{liner}$ versus t or $log(t)$. (a) Monotonic Increasing Pressure Test until failure. The Point A defines the first instability point of the loading curve. The Point B is another instability point. From a security point of view, the Point A is taken as the failure point of the vessel. (b) Monotonic Increasing then Sustained Pressure Tests until failure. After the monotonic part of the pressure loading (time before the vertical bar), the pressure P_{MISPT} was sustained for 4 months (10^7 seconds). The Point A defines the first instability point of the loading curve but it appear that the vessel was far from being separated into two parts. The Point B is another instability point, which does not always correspond to the total destruction of the vessel. From a security point of view, the Point A is taken as the failure point of the vessel. This type of curve can be explained similarly by the experimental measurement made on a simple specimen (Fig. 3): firstly, somewhere in the structure, suddenly, the damage grew but stopped (Point A); then, the time continues and again, somewhere in the structure, suddenly, the damage grew but stopped (Point B) but did not lead immediately to failure.

Figure 10

Representative Volume Element of the material damage states and corresponding i-plets. Broken fibres are in red colour. (a) RVE $CS32$ / 0-plet. (b) RVE $C32$ / 1-plet. (c) RVE $C16$ / 2-plet. (d) RVE $C8$ / 4-plet. (e) RVE $C4$ / 8-plet. (f) RVE $C2$ / 16-plet. (g) RVE $C1$ / 32-plet.

Figure 11

Simple specimen under monotonic loading increasing to failure (ML case). (a) Comparison of loading curves showing the influence of speed of loading. (b) Evolution of the populations of

0-plets and 32-plets (0.02 MPa/s). (c) Evolution of the populations of 0-plets and 32-plets (20.00 MPa/s).

Figure 12

Simple specimen under increasing monotonic loading until held at a constant load until its eventual failure (SL case). (a) Loading curve showing $< e_{11} > / < e_{11} >_{SSL}$ strain in the fibre direction divided by strain at beginning of sustained loading. (b) Evolution of the populations of 0-plets and 32-plets representing clusters of fibre breaks.

Figure 13

Simple specimen under increasing monotonic loading until held at a constant load until its eventual failure (SL case). Scatter of the time-to-failure for different sustained load levels ($X \times F^{MCR001}_{SINST\_20}$, X = 0.96, 0.94, 0.92, 0.90, 0.895, 0.89, 50 Monte-Carlo runs have been considered for each level).

Figure 14

Simple pressure vessel considered for reasons of calculation time. (a) Mesh of the pressure vessel. (b) Mesh of the cross section of the pressure vessel (green: ply 1, 90° / yellow: ply 2, +20° / blue: ply 3, −20° / red: liner).

Figure 15

Simulation of a simplified pressure vessel subjected to increasing monotonic loading up to burst. Comparison of loading curves showing the influence of the speed of loading, as described in full size pressure vessels by Chou *et al.* [9].

Figure 16

Loading curves of MIPT and MISPT cases: average, over the liner, of the radial displacement u_r as a function of the time t, i.e., $< u_r >_{liner}$ (mm) versus $log(t)$. (a) MIPT case. Monotonic increasing pressurization (1 MPa/s) until burst of the vessel. 20 loading curves coming each from one of the 20 different Monte-Carlo runs R_i are plotted. Each of these curves gives a burst pressure $P^{(i)}_{MIPT}$. The burst pressure $P^{(median)}_{MIPT}$ (= 272.45 MPa) is the median value for the burst pressure calculated using a maximum likelihood method for the 20 values $P^{(i)}_{MIPT}$. This value has been taken as the reference for the tests with sustained pressure levels. (b) MISPT case. Monotonic increasing pressurization (1 MPa/s) until $P_{SL} = P^{(J)}_{MISPT}$ equal to X% of $P^{(median)}_{MIPT}$ which was then simulated as being held constant for four months ($\approx 10^7$ seconds). For each value of the sustained pressure, 20 loading curves coming each from one of the 20 different Monte-Carlo runs

R_i (the same as in the MIPT case) are plotted. Each of these curves gives a time-to-failure $t_{MISPT}^{(J/i)}$. (b1) $X = 89.9\%$, $P_{SL} = P_{MISPT}^{(1)} = 245$ MPa. (b2) $X = 91.8\%$, $P_{SL} = P_{MISPT}^{(2)} = 250$ MPa. (b3) $X = 93.6\%$, $P_{SL} = P_{MISPT}^{(3)} = 255$ MPa. (b4) $X = 95.4\%$, $P_{SL} = P_{MISPT}^{(4)} = 260$ MPa. (b5) $X = 97.3\%$, $P_{SL} = P_{MISPT}^{(5)} = 265$ MPa. (b6) $X = 99.1\%$, $P_{SL} = P_{MISPT}^{(6)} = 270$ MPa.

Figure 17

Analysis of the time-to-failure for each value of steady pressure. (a) For each value of steady pressure $P_{SL} = P_{MISPT}^{(J)}$ $(J = 1, ..., 6)$, the twenty values of time-to-failure $t_{MISPT}^{(J/i)}$ were obtained for each Monte-Carlo run R_i $(i = 1, ..., 20)$. The circles indicates the numerical results and the dark lines indicates the scatter obtained with these results. (b) For each value of maintained pressure $P_{SL} = P_{MISPT}^{(J)}$ $(J = 1, ..., 6)$, the twenty values of time-to-failure $t_{MISPT}^{(J/i)}$ allow the parameters of the Weibull distribution $W_{MISPT}^{(J)}$ to be calculated (using the maximum likelihood calculation) for the time-to-failure at this value of steady pressure. In this way, for each value of steady pressure it becomes possible to give the time-to-failure for a choosen probability. The probabilities of failure corresponding to one in a million to one hundred percent certainty have been plotted. (c) For each value of steady pressure $P_{SL} = P_{MISPT}^{(J)}$ $(J = 1, ..., 6)$, the twenty values of time-to-failure obtained have been plotted as well as the smoothed curves of time-to-failure for probabilities from one in a million to one hundred percent.

Figure 18

Ranking in increasing order of the twenty values of time-to-failure obtained for each Monte-Carlo runs for $P_{SL} = P_{MISPT}^{(1)} = 245$ Mpa and $P_{SL} = P_{MISPT}^{(5)} = 265$ Mpa. So that, for example, the R_9 Monte-Carlo run gives the shortest time-to-failure with a pressure of $P_{MISPT}^{(5)} = 265$ Mpa but gives the fifteenth time-to-failure for a pressure of $P_{MISPT}^{(1)} = 245$ Mpa.